Monthly Scientific-Technical and Production Journal

The Paton WELDING JOURNAL

April 2001 # 4

English translation of the monthly «Avtomaticheskaya Svarka» journal published in Russian since 1948

The National Academy of Sciences of Ukraine
The E.O. Paton Electric Welding Institute of the NAS of Ukraine
International Association «Welding»

«The Paton Welding Journal»
is published monthly by the
International Association «Welding»

Promotion group:
V.N.Lipodaev, V.I.Lokteva
A.T.Zelnichenko (Exec. director)
Translators:
S.A.Fomina, I.N.Kutianova,
T.K.Vasilenko

Editorial and advertising offices
are located at PWI,
International Association «Welding»,
11, Bozhenko str., 03680,
Kyiv, Ukraine
Tel.: (38044) 227 67 57
Fax: (38044) 268 04 86
E-mail: tomik@mac.relc.com
E-mail: office@paton.kiev.ua

State Registration Certificate
KV 4790 of 09.01.2001

Subscriptions:
$460, 12 issues, postage included

«The Paton Welding Journal» Website:
http://www.nas.gov.ua/pwj

CONTENTS

SCIENTIFIC AND TECHNICAL

Zamkov V.N., Prilutsky V.P., Petrichenko I.K., Vrzhizhevsky E.L. and **Topolsky V.F.** Effect of the method of fusion welding on properties of welded joints in alloy Ti–6Al–4V 2

Elagin V.P., Snisar V.V., Savitsky M.M., Gordan G.N., Vasiliev V.G. and **Doroshenko L.K.** Chemical and structural inhomogeneity in the zone of fusion of low-carbon steel with austenitic weld during shielded-gas welding 7

Zvyagintseva A.V., Yushchenko K.A. and **Savchenko V.S.** Effect of structural changes in high-temperature heating on ductile characteristics of nickel alloys 13

Vasenin Yu.L., Zagrebelny A.A., Zelnichenko A.T., Krivtsun I.V. and **Shulym V.F.** Modelling of thermal process in piping repair in space 18

Dmitrik V.V. and **Shevchenko V.V.** Effectiveness in use of molten pool heat 24

Goncharov I.A., Paltsevich A.P., Tokarev V.S., Veblaya T.S. and **Kharchenko N.P.** About the form of hydrogen existence in welding fused fluxes 27

Popov S.N. Optimization of chemical composition of deposited metal of components operating under the conditions of abrasive wear 31

INDUSTRIAL

40 years of piloted cosmonautics 34

Lankin Yu.N. and **Gavrish S.S.** Device for provision of safe operation of manual electron beam tool in space 36

Bulatsev K.A. and **Bulatsev A.A.** System of monitoring the position of manual electron beam tool 39

Tochin V.V., Yushchenko B.I., Rusinov P.P., Demianenko V.V. and **Palamarchuk T.E.** Safety system of electron beam tool 41

Prokofiev A.S., Pismenny A.S., Bondarev V.A. and **Bondarev A.V.** Induction braze-welding of no-accessory T-joints in pipes 43

Nesterenko N.P., Senchenkov I.K., Chervinko O.P. and **Dyachenko S.M.** Designing of multistage waveguides-tools for ultrasonic welding of thermoplastic materials 48

Najda V.L., Mozzhukhin A.A., Getman V.V., Pyshny V.M. and **Torop V.M.** Integrated approach in technical diagnostics of pipelines in automatic ultrasonic testing of butt welds 51

BRIEF INFORMATION

Petushkov V.G. and **Titov V.A.** Parameters of shock-wave loading used to relieve residual welding stresses by explosion treatment 56

EFFECT OF THE METHOD OF FUSION WELDING ON PROPERTIES OF WELDED JOINTS IN ALLOY Ti–6Al–4V

V.N. ZAMKOV, V.P. PRILUTSKY, I.K. PETRICHENKO, E.L. VRZHIZHEVSKY and **V.F. TOPOLSKY**
The E.O. Paton Electric Welding Institute, NASU, Kyiv, Ukraine

ABSTRACT

Mechanical and corrosion properties of arc, electron beam and laser welded joints in alloy Ti–6Al–4V are compared, allowing for peculiarities of thermal cycles of laser welding. Susceptibility of the laser weld metal to stress corrosion cracking in an aggressive environment is found to be by an order of magnitude higher than that of the arc weld metal. Annealing of welded joints does not decrease their sensitivity to cracking.

Key words: *arc welding, electron beam welding, laser welding, titanium alloys, mechanical properties, stress corrosion resistance*

The stable trend fixed recently is to extending the field of application of laser welding in aircraft engineering, ship-building, automotive industry, etc. [1 – 5]. The main arguments in favour of replacing arc welding methods by the laser ones include the possibility of dramatically raising productivity (welding speed), reducing (or sometimes even eliminating) amounts of welding consumables, decreasing labour consumption in preparation of edges for welding in making welds on metal of medium thickness and decreasing distortions of welded (especially sheet) structures. At the same time, it should be noted that the number of publications dedicated to evaluation of properties of the laser welded joints in various structural materials, e.g. titanium alloys, is rather small. Laser welding is characterized by extremely high temperature gradients, rates of heating and cooling of the weld and HAZ metal [6 – 8]. Therefore, comprehensive investigations into the effect of rigid thermal cycles inherent in this method on performance of welded joints are required for its successful application.

The purpose of this study consists in comparative investigations of mechanical properties and susceptibility of welded joints in alloy Ti–6Al–4V, made by laser welding, EBW and GTAW over the flux layer [9].

The choice of alloy Ti–6Al–4V as the investigation object is based on the fact that it is widely applied in commercial fabrication of welded structures both abroad (Grade 5) and in the CIS countries (VT6), has good weldability and is well-studied.

Chemical composition and mechanical properties of samples of the base metal used in this study (Tables 1 and 2) indicate that they meet fully the requirements of ASTM and Russian standards for sheet semi-finished products made from alloy Ti–6Al–4V.

Butt joints (Figure 1) of plates 6 × 200 × 300 mm in size were welded using the 5 kW CO_2 laser, UL144 electron beam installation (power unit ELA 60/60) and commercial equipment for GTA welding of titanium. In the latter case the ANT-25A flux was used. Helium was used as the shielding gas in laser welding and argon — in arc welding. In all the cases the welding conditions (Table 3) were selected so that they provided single pass welds without groove preparation. No filler wire was utilized. Results of chemical and gas analyses (see Table 1) showed no changes in the content of alloying elements in the weld metal (independently of the welding method), which was not the case of the base metal. Also, a slight difference in the content of impurities was fixed in the weld metal. Therefore, structure and properties of welded joints made by each welding method depended exclusively on the peculiarities of a heat source and thermal cycle.

Despite the fact that heat input in laser welding was lower by a factor of 3.5 and 4.5 than in EBW and arc welding, respectively, and that the calculated values of the rates of heating and the instantaneous rates of cooling of the weld and HAZ metal differed by an order of magnitude (Table 3), the values of

Table 1. Chemical composition of base and weld metals

Investigation object	*Content of elements, wt.%*						
	Al	*V*	*Fe*	*C*	O_2	N_2	H_2
Base metal	5.54	3.85	0.22	0.10	0.16	0.018	0.0035
Weld metal (arc welding)	5.49	3.82	0.21	0.11	0.17	0.015	0.0042
Same (EBW)	5.61	3.86	0.23	0.10	0.16	0.015	0.0030
Same (laser welding)	5.53	3.81	0.22	0.12	0.18	0.017	0.0064

Table 2. Mechanical properties of base metal*

Direction of cutting out of specimens	*Tensile strength, MPa*	*Yield strength, MPa*	*Reduction in area, %*	*Impact toughness, J/cm²*
Along the rolling direction	1017	968	24	34
Across the rolling direction	1015	968	22	36

*Here and in Table 5 the mean values of tests results on 5 specimens are given.

Table 3. Comparative parameters of thermal effects on base metal in all the welding methods investigated

Parameters	*Welding method*		
	laser	*electron beam*	*arc*
Heat input, J/cm	1350	4800	6000
Width of HAZ, mm ($t > t_{melt}$)	3.1	8.0	16.5
Time of metal dwelling at $t >> t_{melt}$, s	1.65	19	38
Heating rate, °C/s,			
in weld region	~20000	3000	700
at $(\alpha + \beta) \rightarrow \beta$–transition interface	2770	360	150
Cooling rate, °C/s,			
in weld region	1120	530	57
at $(\alpha + \beta) \rightarrow \beta$–transition interface	220	100	11

Note. Width of the HAZ was determined by measurement. The rest of the data were calculated according to [7 – 9].

strength and impact toughness of all of the welded joints had negligible differences and were close to those of the base metal (Tables 2 and 5). What should be noted is just that the laser welded joints had decreased strength values. This is likely to be caused by the peculiarities of phase and structural transformations under conditions of high heating and cooling rates [10], which are characteristic of this process.

Susceptibility of alloy Ti–6Al–4V and its welded joints to corrosion fracture was evaluated on the basis of two properties: resistance to general corrosion in synthetic sea water and resistance to stress corrosion cracking in the CH_3OH + 0.4 % HCl solution. In both cases the tests were conducted at room temperature. It should be noted the HCl content of methanol was in excess of that specified in GOST 9.901.2–89 and GOST 26294–84 for the accelerated corrosion cracking tests of welded joints in titanium alloys.

Results of the tests to susceptibility to general corrosion (Table 6) proved that both alloy and its welded joints (independently of the welding method) were characterized by a high resistance to sea water (according to GOST 13819–68) and had a value of i_c of the same order of magnitude. At the same time, some difference was fixed in the absolute values of

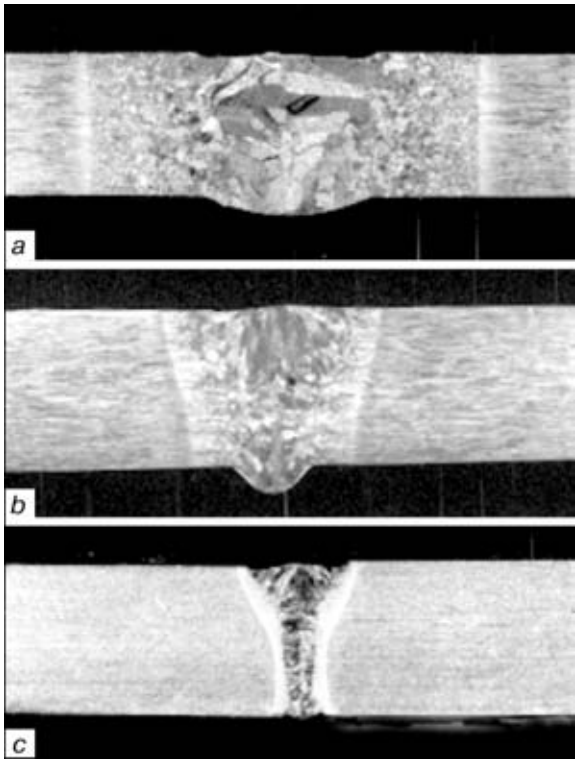

Figure 1. Macrostructure of welded joints made by arc (*a*), electron beam (*b*) and laser welding (*c*)

the rate of corrosion depending upon the welding method. So, i_c of the metal of the isolated zones of the joints made by EBW and laser welding (in contrast to arc welding) and base metal is almost identical (Table 6). The rates of general corrosion, which were determined in the same zones but in the entire welded joints, were much higher. The relative increase in the i_c values for the electron beam and laser welded joints is higher than that for the arc welded joints. It is likely that an increase in the absolute values of i_c measured in the entire welded joints is caused by the

Table 4. Welding conditions and parameters of the welds

Welding method	*Welding current, A*	*Voltage, kV*	*Welding speed, m/h*	*Weld width, mm*		
				top	*middle*	*root*
Arc	210	0.011	9	8.2	6.5	5.7
Electron beam	$8 \cdot 10^{-5}$	60	25	5.8	3.8	2.5
Laser	–	–	75	4.5	1.5	0.8

Note. Laser welding was performed using the 4.5 kW unit.

Table 5. Mechanical properties of welded joints

Welding method	*Tensile strength, MPa*	*Impact toughness, J/cm²*		*Fracture location*
		weld	*HAZ*	
Arc	1019	27	35	Weld
Electron beam	1015	34	32	Weld and base metal
Laser	964	26	31	Weld and HAZ

Table 6. Rates of general corrosion of base and welded joint metals depending upon the welding method, $i_c \cdot 10^{-3}$ mm/year

Investigation object	*Base metal*	*Weld metal*			*HAZ metal*		
		Arc welding	*EBW*	*Laser welding*	*Arc welding*	*EBW*	*Laser welding*
Isolated zones of welded joint*	1.9	2.5	2.1	1.8	2.7	2.3	2.0
Entire welded joint**	3.9	4.3	4.6	4.6	5.1	5.0	5.5

*Weld, HAZ and base metals were cut out from a welded joint.
**Resistance of zones of the entire welded joint was tested using a pressure electrochemical cell.

Table 7. Resistance of alloy Ti–6Al–4V and its welded joints to stress corrosion cracking

Investigation object	*Time of tests, h*	
	Without annealing	*Annealing, 750 °C, 1 h*
Base metal (as-received)	165*, 1050, 1050	1050, 1050, 1050
Welded joint (arc welding)	290*, 650, 670, 1320, 1320	1320, 1320, 1320
Same (EBW)	17*, 90*, 45*, 83*	114*, 135*, 65*, 120*
Same (laser welding)	3*, 4*, 2*, 4*	12*, 17*, 14*

*Specimens cracked in the indicated period of time.

mutual effect of the individual regions of a joint on each other and is associated first of all with the level of locality and character of residual stresses in the entire joint. As the locality of residual stresses in the joints made by EBW and especially laser welding is higher than in the arc welded joints, they have a higher relative increase in i_c.

Results of tests of the base and welded joint metals to stress corrosion cracking (Table 7) were another proof of the known postulates of causes determining sensitivity of alloy Ti–6Al–4V to this type of fracture. As crack resistance of titanium alloys in an aggressive environment depends upon the presence, level and degree of localization of internal stresses in metal, in addition to its structural state and chemical homogeneity [11, 12], the welded joints which as a rule have residual stresses and concentrational heterogeneity (independently of the welding method) are more susceptible to cracking [11, 13, 14]. Under conditions of tensile stresses in an aggressive environment, cracks in ($\alpha + \beta$)-titanium alloys, and in Ti–6Al–4V in particular, are formed along the grain boundaries and at interfaces between the phases [13], and their propagation is caused by formation of titanium hydrides at the crack apex due to hydrogen diffusion [15].

Other conditions being equal, susceptibility to crack initiation and propagation depends upon the relative percentage of the α- and β-phases in the metal, their sizes and morphology. The higher the volume

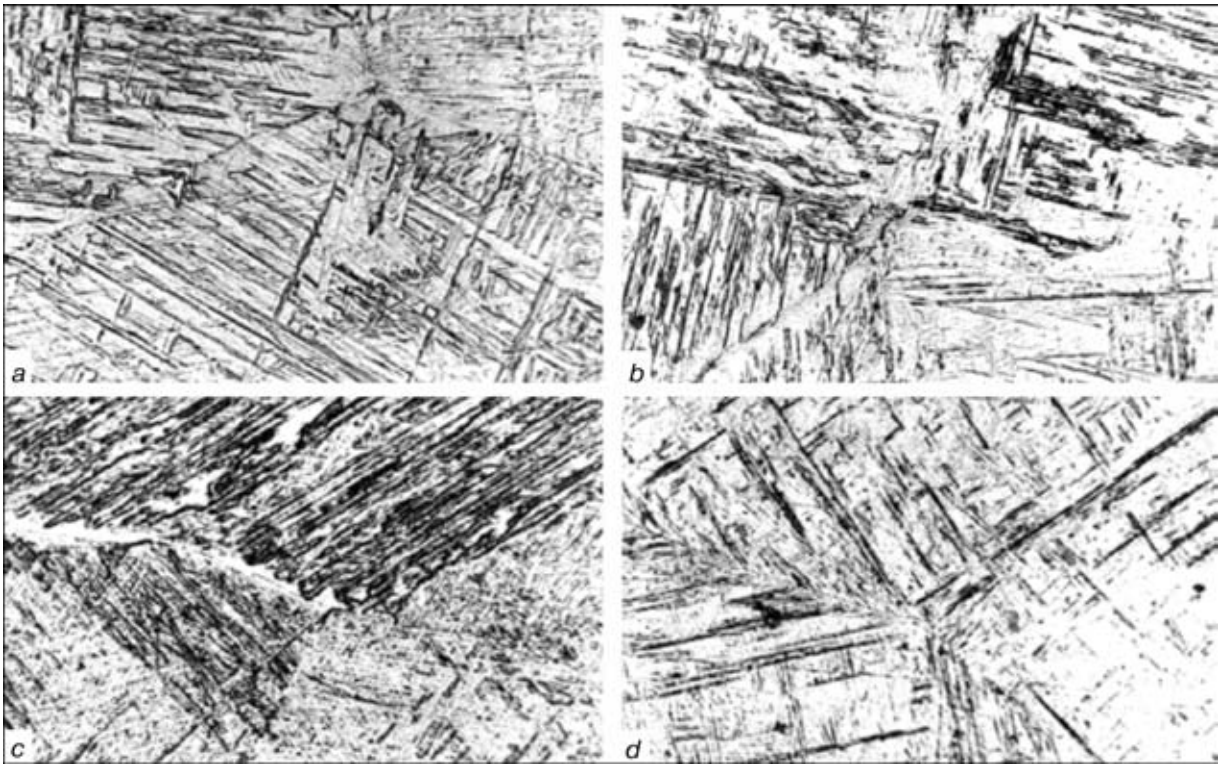

Figure 2. Microstructure of the weld metal made by arc (*a*), electron beam (*b*), same after annealing (*c*) and laser welding (*d*) (×400) (reduced by 4/5)

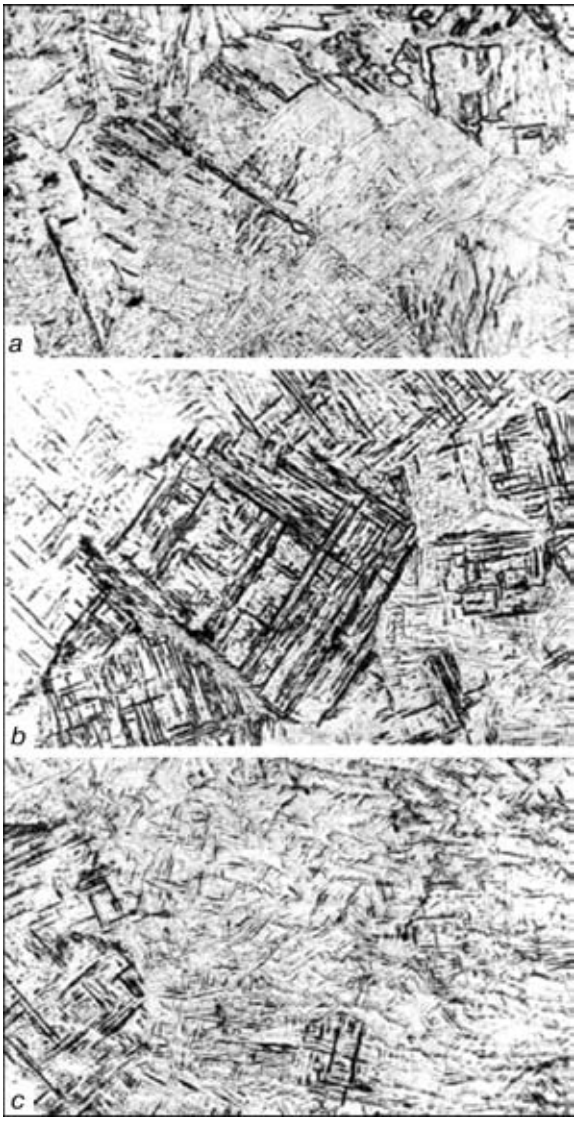

Figure 3. Microstructure of the HAZ metal in the joints made by arc (*a*), electron beam (*b*) and laser welding (*c*) (×400) (reduced by 4/5)

percent of the β-phase and the higher the degree of its dispersion, the more resistant the (α + β)-alloy is to corrosion cracking. Crack resistance of the alloy also increases if the α-phase has a laminated structure [13, 15, 16].

Therefore, the data given in Table 7 are indicative of a rather high crack resistance of alloy Ti–6Al–4V. Besides, despite the fact that the test results on the base metal in the as-received condition were characterized by a substantial scatter, after annealing (750 °C, 1 h) all the specimens withstood the tests for 45 days, showing no indications of cracks. Welded joints made by arc welding over the flux layer exhibited the similar resistance to stress corrosion cracking and its dependence upon annealing. It is likely that the positive effect of annealing in both cases is associated with relief of residual stresses after rolling (in base metal) and after welding (in welded joints), since annealing caused no substantial changes in a microstructure of the metal. In particular, no changes

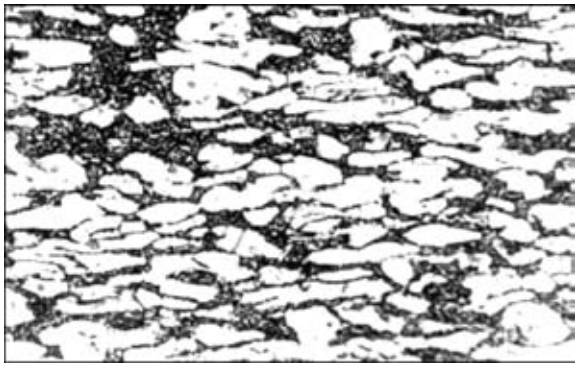

Figure 4. Microstructure of the base metal (×400) (reduced by 4/5)

were detected in shape or thickness of the α-laminae (see Figure 2, *b, c*).

At the same time, annealing had but a slight effect on corrosion cracking of the electron beam and laser welded joints. This suggests that their low stress corrosion resistance is associated primarily with peculiarities of a microstructure of the weld and HAZ metal, which are caused by rigid thermal cycles. Thus, the intra-granular structure of the laser and electron beam weld metals is characterized by a needle-like morphology of the decomposition products formed at the high rates of cooling from the β-region (see Figure 2). Thickness of the needles of the α-phase in them is several times as low as that of the α-precipitates in the weld metal made by arc welding, the size of the primary β-grains being much smaller as well. The needle-like structure of the α-phase persisted also after annealing, although some changes did take place in the needles and in the matrix during their decomposition. A distinctive feature of microstructure of the weld regions of the HAZ in the joints made by laser welding is the absence of the grain growth (Figure 3, *c*). Contours of the globular grains of the α-phase characteristic of the base metal (Figure 4) were detected in individual regions, up to the fusion zone. Precipitation of the needles of the martensitic α-phase occurs within the limits of the α-globules. Only isolated recrystallized grains in the HAZ metal showed trend to growth. In general, it should be noted that the methods of optical metallography, except for differences in sizes of structural components, failed to reveal any other essential differences in microstructure of the joints made by EBW and laser welding, which could be responsible for a low resistance of these joints to corrosion cracking.

In addition to morphology and dispersion of structural components, the character of fracture of (α + + β)-titanium alloys may be considerably affected by a dislocation structure [17, 18].

CONCLUSIONS

1. Mechanical properties of welded joints in alloy Ti–6Al–4V, made GTAW over the flux layer, EBW and laser welding, are at the same level and close to the corresponding properties of the base metal.

2. Independently of the welding method, the welded joint and base metals are characterized by a high resistance to general corrosion in sea water. The rates of corrosion of the weld, HAZ and base metals are of the same order of magnitude and close to each other in absolute values.

3. Laser welded joints are characterized by a minimum stress corrosion resistance (by two orders of magnitude lower than that of the base metal) both in the as-welded condition and after annealing. GTAW over the flux layer provides crack resistance of the welded joints equal to that of the base metal. The electron beam welded joints take an intermediate position.

4. Detailed investigations into peculiarities of the metal microstructure formed under conditions of the thermal cycles characteristic of laser welding are required to find out the causes of susceptibility of the laser welded joints to stress corrosion cracking.

REFERENCES

1. Schutte, M. (1995) European laser market — place'94. *Blech Rohre Profile*, **2**, 115 – 116.
2. Irving, B. (1994) What's the latest news on laser beam welding and cutting? *Welding J.*, **26**, 34 – 35.
3. Cam, G., Dos Santos, I.F., Kosak, M. (1997) Laser and electron beam welding of Ti-alloys. Literature review. *GKSS /Rept.*, **35**, 1 – 26.
4. Seyffarth, P. (1996) State-of-the-art and trends of development in the field of laser sources of treatment. In: *Proc. of Int. Sci.-Techn. Conf. on Welding in Power Generation,* Kyiv, Oct. 2 – 3. Kyiv.
5. Leuschen, V., Spies, B. (1994) Stand und Entwicklungsten denzen des Laserstrahlschweißens und -schneidens im Automobilbau. In: *Sammlung der Vorträge Aachener Schweisstechn. Kolloq.*, Juni 10. Aachen.
6. Rykalin, N.N., Uglov, A.A., Zuev, I.V. *et al.* (1975) *Laser treatment of materials*. Moscow: Mashinostroyeniye.
7. Rykalin, N.N., Uglov, A.A., Zuev, I.V. *et al.* (1985) *Laser and electron beam treatment of materials*. Refer. Book. Moscow: Mashinostroyeniye.
8. Grigoriants, A.G., Shiganov, I.N. (1988) *Laser welding of metals*. Moscow: Vysshaya Shkola.
9. Paton, B.E., Zamkov, V.N., Prilutsky, V.P. (1998) Le soudage A-TIG du titane et de ses alliages. *Soudage et Techniques Connexes*, **11/12**, 23 – 26.
10. Ivasishin, O.M., Oshkaderov, S.P. (1982) Effect of the rate of heating for quenching on structure of alloys VT23 and VT6. *Metallovedeniye i Term. Obrab. Metallov*, **7**, 14 – 16.
11. Shelenkov, G.M., Blashchuk, V.E., Melekhov, R.K. (1984) *Manufacture and operation of titanium equipment*. Kyiv: Tekhnika.
12. Mashino, S., Noriya, T., Suzuki, H. *et al.* (1991) Investigation of the mechanism of microstructure of alloy Ti–6Al–4V with an acicular structure by the acoustic emission method. *J. Jap. Inst. Metals*, **7**, 756 – 764.
13. Tsviker, U. (1979) *Titanium and its alloys*. Moscow: Metallurgia.
14. Moroz, L.S., Chechulin, B.B., Polin, I.V. *et al.* (1960) *Titanium and its alloys*. Leningrad: Sudpromgiz.
15. Chechulin, B.B., Khesin, Yu.D. (1987) *Cyclic and corrosion strength of titanium alloys*. Moscow: Metallurgia.
16. Fedotov, A.S. (1984) Principles of fracture of two-phase titanium alloys with different microstructure. *Metallovedeniye i Term. Obrab. Metallov*, **5**, 55 – 57.
17. Tomsinsky, V.S., Shishkina, M.I., Bezrukova, A.K. *et al.* (1981) Effect of structure on crack resistance of alloy VT3-1. *Ibid.*, **12**, 33 – 34.
18. Anisimova, L.I., Popov, A.A. (1985) Relationship between the character of fracture, microstructure and properties of ($\alpha + \beta$)-titanium alloys. *Ibid.*, **12**, 45 – 48.

EFFECT OF STRUCTURAL CHANGES IN HIGH-TEMPERATURE HEATING ON DUCTILE CHARACTERISTICS OF NICKEL ALLOYS

A.V. ZVYAGINTSEVA, K.A. YUSHCHENKO and **V.S. SAVCHENKO**
The E.O. Paton Electric Welding Institute, NASU, Kyiv, Ukraine

ABSTRACT

Investigation of hot ductility of alloy IN 840 proves that it has three characteristic ductility temperature ranges. Drastic fall in ductility takes place in a narrow temperature range. It results from melting of grain boundaries to form on them small amounts of the liquid films. The data of metallography and fractography obtained on welded samples show that fracture at high temperatures occurs along the boundaries of grains (dendrites) rich in alloying elements and is of the same nature as fracture of the base metal at high temperatures.

Key words: *heat-resistant nickel alloys, hot ductility, fracture mechanism, nil ductility temperature, melting of grain boundaries, chemical heterogeneity, enrichment of boundaries, dendrites*

High-temperature strength and ductility tests are an integral part of investigations to study weldability and properties of metal welded joints. Metallurgical changes taking place during the high-temperature tests are studied to determine more precisely how the data of investigation of strength and ductility correlate with the welding experiments.

Hot ductility is determined by simulating the thermal cycle of metal heating and cooling, i.e. simulating the processes occurring in the HAZ metal during welding. For this the tests are conducted within the selected range of temperatures of the thermal cycle to determine characteristic peculiarities of ductility depending upon the heating temperature. Four regions of changes in hot ductility (Figure 1) can be distinguished on the basis of the test results:

I — ductility is constant with an increase in temperature. The temperature is too low for activation of the diffusion and strengthening processes, therefore, ductility in this region does not depend upon the temperature [1];

II — ductility decreases with further increase in temperature. In this region, the energy of binding of an impurity atom with dislocations being maintained at a sufficiently high level, mobility of the atom increases owing to an increase in the diffusion parameters. Transportation of impurity atoms to the grain boundaries results in an intergranular embrittlement and, thus, the hot ductility dip [2];

III — ductility grows to very high values with further increase in temperature. For nickel alloys this region begins with the strengthening processes being dominated by the weakening ones, i.e. recrystallization, which is attributable to high stresses and high temperatures [1];

IV — very rapid fall of ductility with further increase in temperature. The «nil» ductility and «nil» strength temperatures, which correspond approximately to the solidus and liquidus temperatures of the base metal, belong to this region.

For metal with a stable austenitic structure, within the temperature ranges of regions *I* – *III*, the strength falls gradually and has a bend at the boundary of ranges of regions *III* and *IV*. This bend coincides with the ductility dip temperature.

Region *IV* is of special interest for researchers. Many of them investigated causes of a drastic fall in ductility. However, until now there is no single opinion on this phenomenon.

In [3] a stable austenitic metal IN 600 was selected as the material for investigations. Specimens were tested using the «Gleeble» testing machine. Two series of tests were conducted to describe the thermal cycle: first during heating and second — during cooling. The nil ductility point was the maximum temperature of holding of the test specimens on the cooling branch, simulating the welding cycle.

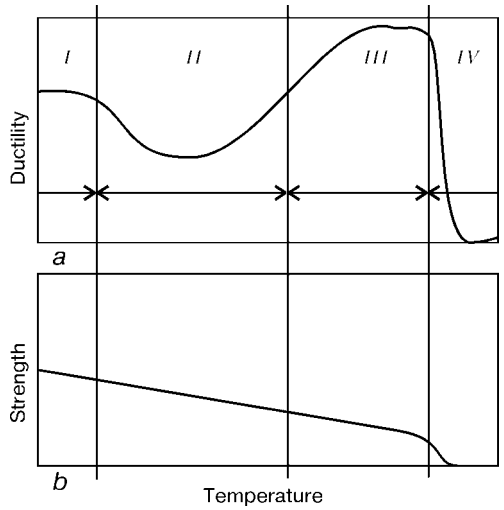

Figure 1. Changes in ductility (*a*) and strength (*b*) of stable austenitic steels depending upon the temperature

Microstructural investigations of specimens tested on the heating branch showed the presence of the serrated grain boundaries, terrace-like fracture surface, partial change in the kind of fracture from tough to brittle and segregated precipitates. According to the model presented, the presence of these changes is caused by partial melting at the grain boundaries. Investigations conducted in [3] at the cooling branch show that during cooling of the specimens, which were preliminarily heated to a solid-liquid state temperature, the region of the liquid grain boundaries is crystallized in a preferred orientation <111>, the dissolved impurities diffusing from the zones near the boundaries into the formed liquid. This growth is proved by the presence of the serrated grain boundaries and the terrace-like surface structures.

According to the data given in [4], the ductility dip is associated with an incipient melting at the grain boundaries, the bend in strength is attributable to the formation of films of critical thickness and the nil strength is indicative of the presence of several percent of a molten volume.

In [5], nickel alloy IN 738 subjected to three different types of heat treatment was used as an example to study variations in microstructure during simulation of the welding thermal cycle using the «Gleeble» testing machine and relationship between variations in microstructure and loss in ductility. It was found that growth of grain, recrystallization and dissolution of impurities had no effect on the ductility loss.

Investigated were specimens subjected to three different types of heat treatment: as-received, subjected to ageing and solution treated. All structures exhibited liquation of boundaries above the nil ductility temperature. The test data on the cooling branch showed that ductility remained low from a maximum temperature to the temperature approximately equal to that of the nil ductility obtained on the heating branch. The test data also showed that at the temperature of beginning of melting the microstructure formed the intergranular liquid in the same way in all three types of heat treatment.

The problem of an adequate determination of the ductile properties at high temperatures is considered also in [6]. The tests were performed using equipment in which the induction coil was located around a specimen prepared for the tests, which allowed melting of part of the test specimen. Molten metal was retained in place by surface tension forces. A thermocouple was placed inside the specimen and was isolated from it by a ceramic coating. All the tensile tests, like in the previous cases, showed a fundamental fall in elongation within a narrow temperature range. The authors attribute the strength above the minimum ductility dip temperature to the presence of capillary forces due to thin films connecting the crystals. Owing to a thin layer of liquid between solid parts, fracture in the ductility dip temperature range looks sometimes smooth and sometimes serrated.

Analysis of the published data shows that the majority of the criteria used for prediction of behaviour of metal during welding are based on mechanical characteristics (reduction in area and (or) strength), whereas there is no single opinion as to interpretation of the microstructural peculiarities.

It was of interest to conduct investigations to study the ductility dip conditions within a narrow temperature range and their relationship with microstructural changes in simulation of the welding cycle. In this study the investigations were conducted on specimens of nickel alloy IN 840 with the following content of base and impurity elements, wt. %: C — 0.025; Mn — 0.39; Fe — 58.04; Cr — 20.15; Ni — 18.91; Ti — 0.42; Al — 0.40; Mo — 0.11; N — 0.016; O — 0.003; Ca — 0.001; S — 0.002; P — 0.0084; Si — 0.63.

The tests were performed using the «Ala-Too» testing machine of the «Gleeble» type within a temperature range of 20 to 1380 °C, with a work vacuum chamber under a residual pressure of $6.6 \cdot 10^{-4}$ Pa. The specimens were heated by the radiation method using a tantalum heater. The temperature was regulated and maintained by means of an automatic potentiometer using a platinum to platinum–rhodium thermocouple welded by the capacitor-discharge method to a gauge length of each specimen. Upon reaching the selected temperature and holding for a few minutes, the specimens were fractured at a rate of $1.83 \cdot 10^{-3}$ s^{-1}.

The ductility characteristic, i.e. reduction in area ψ, which was determined from the following formula:

$$\psi = \frac{l - l_0}{l_0} \cdot 100\%,$$

where l_0 and l is the thickness of the specimen before and after the test, respectively, was used as the criterion of evaluation of the ductile properties.

Investigation of distribution of elements in the welds and fractography were carried out using the JEOL scanning electron microscope of the YSM T-200 type (Japan) and the Camebax microanalyser of the SX50 type (France).

Sections for metallography were etched using the VUP-4 unit by the vacuum ion etching method.

Behaviour of metal in the solid-liquid state and weldability were investigated by the Varestraint test method to provide dynamic deformation of a welded joint. Allowing for an insignificant thickness of the materials under investigation, which was much less than thickness of the plates recommended for investigations by the Varestraint test method, a welded sample was made from stainless steel of the 08Kh17T (C — 0.08; Cr — 17.0; Ti — 1.0 wt.%; Fe — balance) type 3 mm thick, to which a strip of the composition investigated was welded. Welding during the tests was done by the GTAW method at a current of 70 A and speed of 0.6 m/min. The test consisted in deformation of the weld metal by bending using a series of mandrels with different radius. The time of deformation was 0.04 s. At the moment of deformation

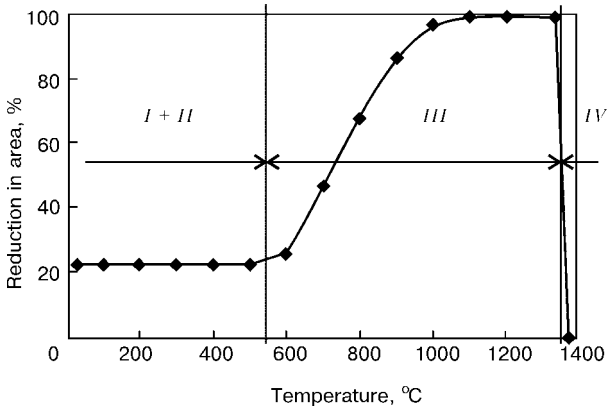

Figure 2. Dependence of reduction in area upon the test temperature for alloy IN 840

the welding was not stopped, but was continued for some time.

The curve (Figure 2) was plotted by the results of the hot ductility tests. The curve can be conditionally subdivided into three regions:

I + II — from room temperature to 700 °C, in which elongation increases but slightly;

III — from 700 to 1340 °C, where elongation dramatically grows;

IV — above 1340 °C, where elongation falls very rapidly to zero.

To study processes which occur in the material at the moment of a fundamental fall of elongation within a narrow temperature range, the fracture surfaces of the specimens tested at temperatures which were the closest to the conditional boundary between regions *III* and *IV* on the ductility curve were investigated by scanning electron microscopy. As shown by the results, the fracture surface of the specimen from region *III*, tested at a temperature of 1340 °C, has the form characteristic of tough fracture (Figure 3, *b*). It can be seen that its fracture surface has a cellular structure which accompanies the deformation process. In this case the temperature does not yet reach the values at which the grain boundaries start melting, and the crack propagates in the bulk of grain, rather than along its boundaries.

The specimen from region *IV* was tested at a temperature of 1380 °C. Figure 3, *c* shows thickened boundaries, as compared with boundaries of the specimen from region *III* (Figure 3, *a*), the formation of which is associated with the beginning of melting. Fracture (Figure 3, *d*) looks smooth and intergranular. The presence of characteristic fragments of crystallization at the fracture surface is also indicative of the beginning of melting, coinciding with the ductility loss. Such a change in the fracture surface can be explained as follows: small tears are formed at the boundary between the neighbouring grains, they lead to an increase in local stresses to provoke formation of local fractures. The crack under such conditions propagates along the boundaries of the grains «bridged» by a molten material formed between the crystals.

The data of energy dispersion analysis of the fracture surface show that brittle fracture results in an

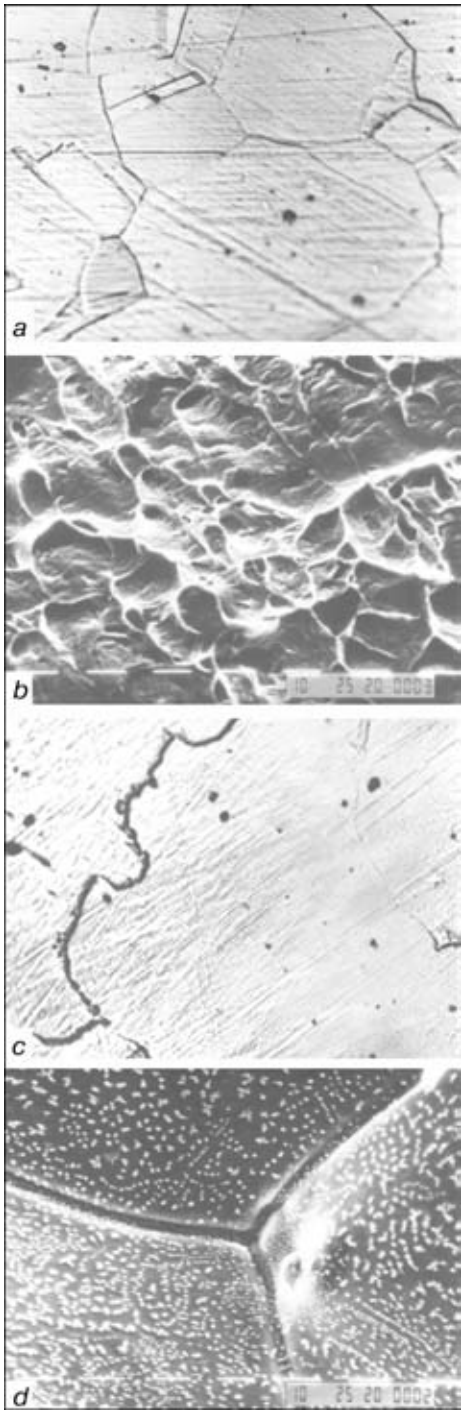

Figure 3. Microstructure (*a, c*) (×400) and fractography of the surface of alloy IN 840 (*b, d*) (×500) at test temperatures of 1340 (*a, b*) and 1380 °C (*c, d*)

increase in the amount of sulphur, aluminium and titanium on the fracture surface (Figure 4). These compounds favour beginning of melting along the grain boundaries, being one of the causes of the ductility dip.

Enrichment of the fracture surface with titanium, sulphur and aluminium is caused by several factors: being characterized by high diffusion parameters (Q — activation energy, J·mole^{-1}, and D_0 — diffusion coefficient, cm^2·s^{-1}) and having a limited solubility in the matrix, these elements diffuse to the grain boundaries and are accumulated there [2]. The

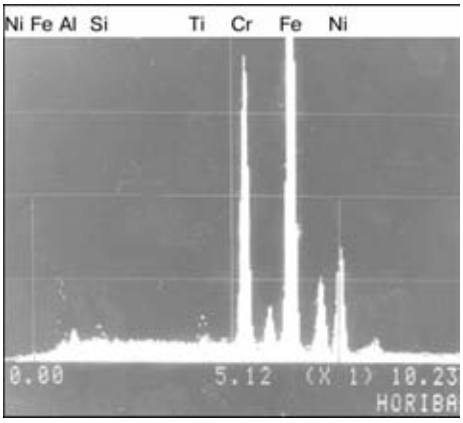

Figure 4. Qualitative energy dispersion analysis of the fracture surface of samples of alloy IN 840

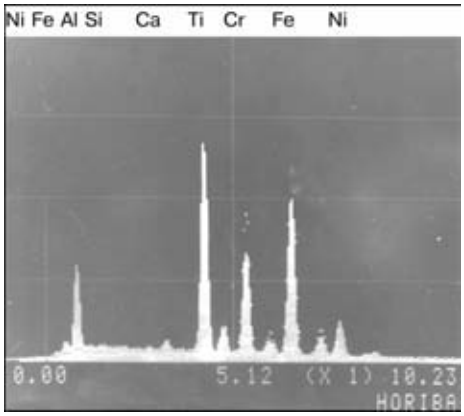

Figure 6. Local chemical composition of the enriched zone at the surface of a hot crack in the IN 840 welds

temperature of melting of the boundaries enriched with these elements is lower than the temperature of melting of the body of grain. After formation of liquid regions at the grain boundaries, the difference in the solubility coefficients of such elements as aluminium, titanium and sulphur favours further accumulation of the said elements in the liquid phase along the boundaries, whereas the grain body is still in the solid state.

Therefore, investigation of the hot ductility of heat-resistant alloys using the «Ala-Too» testing machine proved the presence of three characteristic ductility temperature ranges.

Our data on investigation of the fracture surface show that the ductility dip within a narrow temperature range occurs as a result of melting at the grain boundaries and formation on them of small volumes of the liquid films, and that an increase in the amount of the liquid phase leads to the fall of ductility to zero.

The tests conducted using the Varestraint test machine show that the weld metal adjoining the liquid pool and being in the solid-liquid state is susceptible to formation of transverse hot cracks.

Investigation of an element composition of the surface in a region of the weld centre using the energy dispersion analyser of the JEOL scanning electron microscope showed the presence of chemical heterogeneity in the metal structure. Besides, the investigations revealed enrichment of the interdendritic zones with such elements as aluminium, silicon, sulphur, potassium and calcium (Figure 5). Fractography patterns of the opened crack revealed the enrichment zone with indications of a brittle fracture being present in the subsurface layer. Investigation of the element composition of the surface of this region by the energy dispersion analysis method showed enrichment of the surface with silicon and especially with titanium (Figure 6). Optical metallography proved development of intergranular and interdendritic heterogeneity of the structure (Figure 7), which was formed as a result of the liquation process taking place during solidification of the weld metal. This can be seen from a change in a range of colour of structural components of the metal. The character of crack propagation investigated by optical metallography is shown in Figure 8. It can be stated that hot cracks are located in the interdendritic enrichment zones. This is proved by measurements of chemical heterogeneity in the crack zone indicated by an arrow in Figure 8. The investigations were conducted using the Camebax analyser by the titanium and silicon elements which enriched the interdendritic zones, according to the energy dispersion analysis data. Results of measurements of the zone indicated by the arrow in Figure 8 are shown in Figure 9. Analysis proves the enrichment of the indicated region with titanium, silicon and nickel.

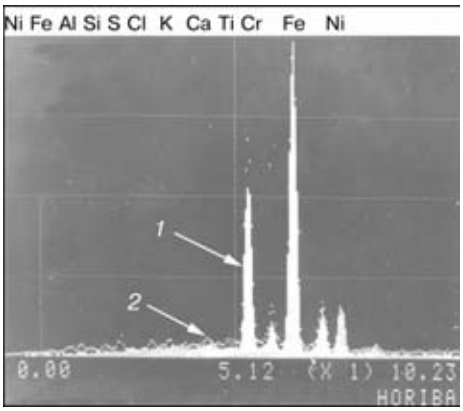

Figure 5. Chemical composition of the primary axis of dendrite in the central part of the surface of the IN 840 weld (curve *1*) with the superposed curve *2* of composition of the interdendritic regions

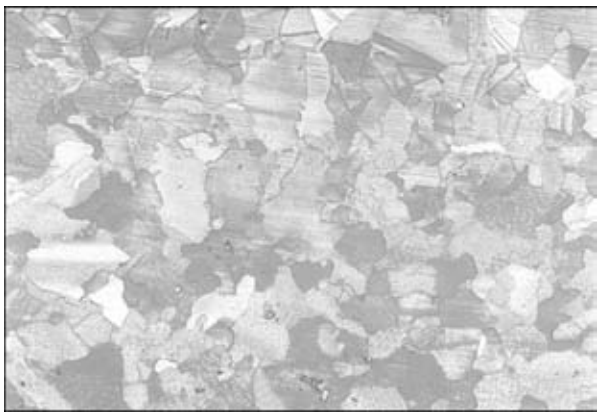

Figure 7. Microstructure of the joint in alloy IN 840 (×200) (reduced by 2/5)

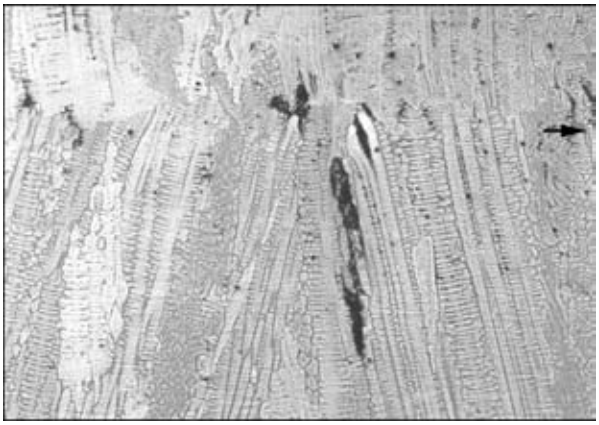

Figure 8. Hot cracks in the IN 840 welds (×200) (reduced by 2/5)

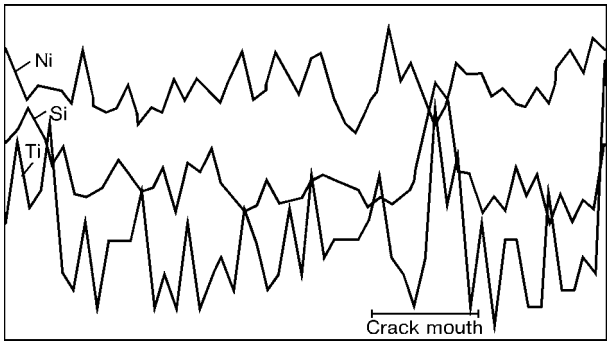

Figure 9. Data of measurements of chemical heterogeneity in the crack zone indicated by arrow in Figure 8

Therefore, the metallography and fractography data obtained using the Varestraint test machine on the welded samples correlate with the data obtained using the «Ala-Too» machine for the base metal, and are indicative of the fact that fracture at high temperatures occurs along the boundaries of the grains (dendrites) rich in alloying elements.

CONCLUSIONS

1. Investigation of hot ductility of heat-resistant alloys using the «Ala-Too» testing machine by an example of nickel alloy IN 840 proved the presence of three ductility temperature ranges and a drastic fall in ductility in a narrow temperature range, which occurred as a result of incipient melting of the grain boundaries to form on them small amounts of the liquid films, leading to a change in the fracture mechanism.

2. Fracture of the welded samples in nickel alloy at high temperatures occurs along the boundaries of the grains (dendrites) enriched with alloying elements, and is of the same nature as fracture of the base metal at high temperatures.

3. Behaviour of alloy IN 840 in cooling from the solid-liquid state temperatures and behaviour of the grain boundaries in solidification and during a drastic change in strength and ductility require additional studies.

REFERENCES

1. (1995) *Superalloys II.* Ed. by C.H. Siems, N.S. Stoloff, W.K. Hargel. Moscow: Metallurgia.
2. Savchenko, V.S., Yushchenko, K.A. (1993) Mechanism of formation and ways for elimination of underbead cracks in welding austenitic steels. *Avtomaticheskaya Svarka*, **2**, 8 – 11.
3. Weiss, B., Krotke, G.E., Sticker, R. (1970) Physical metallurgy of hot ductility testing. *Welding Research Suppl.*, **10**, 471.
4. Lee, C.H., Lundin, C.D. (1998) Relationship between hot ductility behaviour and microstructural changes in TP347 stainless steel. *Welding J.*, **1**, 29 – 37.
5. Thompson, R.G., Genculu, S. (1983) Microstructural evolution of the HAZ of Inconel 718 and correlation with the hot ductility test. *Ibid.*, **12**, 337 – 345.
6. Bo, R. (1983) An investigation of the hot ductility of steels by performing tensile test on «in situ solidified» samples. *Scand. J. of Met.*, **12**, 51 – 66.

MODELLING OF THERMAL PROCESS IN PIPING REPAIR IN SPACE

Yu.L. VASENIN, A.A. ZAGREBELNY, A.T. ZELNICHENKO, I.V. KRIVTSUN and **V.F. SHULYM**
The E.O. Paton Electric Welding Institute, NASU, Kyiv, Ukraine

ABSTRACT

A mathematical model of thermal processes in welding of piping in space is proposed. Software has been developed for implementation of the above model in the computer. Detailed computer simulation of thermal processes in stainless tube brazing has been performed. Optimal geometrical parameters and conditions of the brazed joint heating are determined, as well as time and energy required for performance of brazing.

Key words: *space, space vehicle, repair, piping, brazing, braze alloy, thermal processes, temperature field, fusion, simulation, investigations*

One of the major problems facing the aerospace experts, is ensuring the service life of the space vehicle and its service systems, envisaging normal operation of a quite expensive item for several years (satellites for various purposes and interplanetary vehicles), or even decades (orbital stations and production facilities on other planets). This problem is being currently solved in two ways [1]:

- development of advanced materials and new components, respectively, incorporating them into the designs of the promising space vehicles;
- provision of space vehicle repairability under their service conditions.

It is understandable that the optimal solution of the repair problem is replacement of failing modules or complete systems. This, however, is not always feasible and is always expensive. Therefore, the well-established methods of individual component repair should not be discarded, this being especially effective in the case of an emergency failure of any component, for instance, in the space vehicle life support system. In this case, it is proper to make a comparison to the orbital stations and modern nuclear submarines that for months are at sea on their own and are fitted with workshops having machining and welding equipment, as well as a wide range of tools.

The urgency of the problem of ensuring repair of the long-term space vehicles, became particularly obvious over the last years of «Mir» orbital station operation. By the data of experts, responsible for maintenance of the station operability, approximately 50 % of the work performed in the station, were related to repair and restoration of its various system functions.

One of the vulnerable, but also the most vital life support sections in such complexes, is the many kilometer piping (steel, titanium, aluminium) for various purposes. The ability to repair the failing tube by its simple replacement seems improbable (especially, in an emergency). In this case, it is almost impossible to do without the traditional methods of joining materials by welding and brazing processes.

The subject of this study is investigation of thermal processes in repair of space vehicle piping by the brazing process in space. Solving this task will permit determination of the most effective process parameters of the future standard on-board hardware to implement the above process, allowing the long-term vehicle piping system repair to be performed by the crew little or not at all skilled in this profession.

The schematic suggested by academician B.E. Paton is the simplest one for making the joint in brazing of piping in space (Figure 1). According to this schematic, the damaged piping section is replaced by a tubular insert of the same material, having appropriate length, outer and inner diameters. The insert is centered relative to the piping axis using two couplings (just one of them is shown in the drawing) that are moved off the insert by half of their length towards the solid sections of the piping, after the insert has been placed into the piping rupture. Then a heat source distributed over the outer surface of the coupling, as shown in Figure 1, is used to heat the item up to complete melting of the braze alloy, earlier deposited onto the coupling inner surface, its filling the part of the gap between the piping and the coupling and, finally, reaching the brazing temperature in the zone of contact of the braze alloy with the outer surface of the insert and the piping*. This results in formation of the brazed joint.

This paper is devoted to development of a mathematical model and detailed computer modelling of thermal processes in brazing of stainless steel piping in space. The aim of modelling is determination of the optimal geometrical dimensions of the coupling and selection of its material, thickness of the layer of the braze alloy required for deposition on its inner surface, as well as optimal conditions and time of the item heating to provide a sound brazed joint.

*The given schematic of brazing the joint is conditional, the actual design variant of the above component should provide complete filling of the gap with the molten braze alloy and fillet formation.

Mathematical model. A non-stationary quasi linear equation of heat conductivity will be used for calculation of the temperature field in all the components of the joint (areas *1* – *4* (*4′*) in Figure 1) in the considered method of repair of the space vehicle piping. Taking into account the azimuthal symmetry of the system, this equation for each of the above areas $D_i (i = 1, \ldots, 4, 4')$ in the cylindrical system of co-ordinates (see Figure 1) can be written in the form of

$$\rho_i C_i \frac{\partial T_i}{\partial t} = \frac{1}{r}\frac{\partial}{\partial r}\left(r\lambda_i \frac{\partial T_i}{\partial r}\right) + \frac{\partial}{\partial z}\left(\lambda_i \frac{\partial T_i}{\partial z}\right), \quad r, z \in D_i, \quad t > 0. \tag{1}$$

Here, $T_i(r, z, t)$ is the space-time distribution of temperature in i-th region ($i = 1, \ldots, 4, 4'$); $\rho_i(T)$ is the density; $\lambda_i(T)$ is the heat conductivity coefficient; $C_i(T)$ is effective heat capacity of the appropriate material that is determined allowing for the heat of it melting:

$$C_i(T) = c_i(T) + W_{mi}\,\delta(T - T_{mi}), \tag{2}$$

where $c_i(T)$ is the specific heat; W_{mi} is the latent heat of melting; T_{mi} is the material melting temperature in i-th region.

Assuming the insert length to be large enough and the coupling position symmetrical relative to the plane of contact of the insert with the main piping (plane $z = 0$ in Figure 1), the temperature field can also be assumed to be symmetrical relative to the above plane. In this case in section from the start of heating up to complete melting of the braze alloy, equation (1) can be solved only in three of the four considered areas, for instance, in region *1* and in the upper halves of regions *3* and *4* (see Figure 1).

$$\begin{aligned} D_1 &= \{r : R_1 - \delta_1 < r < R_1,\ 0 < z < L_1\}, \\ D_3 &= \{r : R_2 < r < R_2 + \delta_2,\ z : 0 < z < L/2\}, \\ D_4 &= \{r : R_2 - \Delta < r < R_2,\ z : 0 < z < L/2\}, \end{aligned} \tag{3}$$

where R_1 is the outer radius of the piping and the insert; δ_1 is their wall thickness; R_2 is the inner radius of the coupling; δ_2 is its wall thickness; L is the coupling length; Δ is the thickness of the initial layer of the braze alloy. Let us assume that after assembly of the joint under consideration, there is a gap of a finite width between the piping external surface and inner surface of the braze alloy layer. Considering that brazing is performed under zero gravity, i.e. in the absence of the convective component of heat exchange between the above surfaces, the heat exchange between the piping and the coupling at the initial stages of the joint heating is considered as just radiation heat exchange [2]. In the case when brazing is performed inside the space vehicle living compartments, i.e. at atmospheric pressure, in addition to radiation heat exchange, the conductive component of heat exchange, related to heat conductivity of the air present in the gap, should be also taken into account.

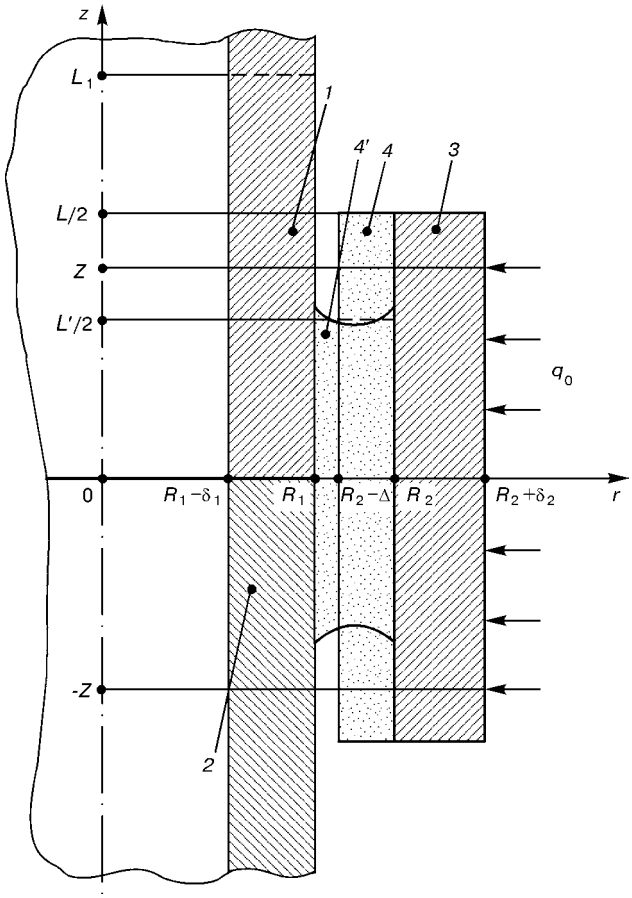

Figure 1. Schematic of a brazed joint in repair of the space vehicle piping: *1* — piping; *2* — insert; *3* — coupling; *4* — initial layer of the braze alloy; *5* — braze alloy melt (for other designations see the text)

When solving the heat conductivity equations, we assume that after the braze alloy melting temperature (liquidus) has been reached in all the points of region D_4, it changes its shape under the impact of surface tension forces and fills the gap between the coupling inner surface and the outer surface of the piping, as shown in Figure 1. In further solution of the system of equations (1), let us approximately consider area D_4' as the area having a rectangular cross-section, that can be defined as follows under the condition of preservation of the braze alloy volume (see Figure 1):

$$D_4' = \{r : R_1 < r < R_2,\ z : 0 < z < L'/2\}, \tag{4}$$

where, provided condition $\Delta << R_2$ is satisfied for the length of this region L', we have

$$L' \approx L\,\frac{2\Delta/R_2}{1 - (R_1/R_2)^2}. \tag{5}$$

It is further assumed that after the braze alloy contact with the piping surface at $z < L'/2$, an ideal thermal contact between regions D_1 and D_4' is established.

Let us assign the initial and boundary conditions for solving equations (1) in the considered areas. Let us select the obvious condition as the initial one

$$T_i\,|_{\,t=0} = T_a, \tag{6}$$

where T_a is the ambient temperature. The boundary conditions for equations (1) are assigned, proceeding from the following considerations. As it is assumed that the temperature field is symmetrical relative to plane $z = 0$, boundary conditions for temperature in all areas at $z = 0$ are selected in the form of conditions of solution symmetry. On the inner boundary of region D_1 it can be assumed that

$$\frac{\partial T_1}{\partial r}\Big|_{r = R_1 - \delta_1} = 0, \qquad (7)$$

as under zero gravity conditions, the convective heat exchange is absent, and radiation heat exchange between the regions of the inner surface at a slow change of its temperature in the longitudinal direction, can be neglected. On the boundary of region D_1 that is opposite to plane z = 0, we assume that

$$T_1\big|_{z = L_1} = T_a. \qquad (8)$$

Here, L_1 is the length of region D_1, selected to be so large that with its further increase, the change of the temperature field in the zone of the joint heating becomes negligible. On the piping outer surface beyond the coupling ($z < L/2$) conditions of radiation heat exchange with the environment are assigned:

$$\lambda_1 \frac{\partial T_1}{\partial r}\Big|_{r = R_1} = \varepsilon_1 \sigma_0 \left(T_a^4 - T_1^4\big|_{r = R_1}\right), \qquad (9)$$

where ε_1 is the degree of the piping material blackness; σ_0 is Stefan–Boltsmann constant. As it is assumed that assembly of the joint results in a gap of a finite width between the coupling and the piping surface, transparent for thermal radiation, at the initial stages of heating (up to the braze alloy melting) the boundary conditions on the outer boundary of region D_1 at $0 < z < L/2$ are taken in the form similar to (9) with replacement of T_a by $T_4\big|_{r = R_2 - \Delta}$ and of ε_1 by the reduced degree of blackness $\bar{\varepsilon}_{1,4}$, calculated by the equation from [2]:

$$\bar{\varepsilon}_{1,4} = \frac{\varepsilon_1 \varepsilon_4}{\varepsilon_1 + \varepsilon_4 - \varepsilon_1 \varepsilon_4}, \qquad (10)$$

where ε_4 is the degree of blackness of the braze alloy material. After part of the gap has been filled with the braze alloy, the boundary condition in the zone of the braze alloy contact with the piping surface, i.e. at $0 < z < L'/2$ is replaced by the condition of an ideal thermal contact. It is assumed that on the remaining part of the piping surface that is under the coupling, the conditions for radiation heat exchange with the coupling inner surface are still satisfied.

Let us assign boundary conditions for region D_3 (see Figure 1) as follows. On the coupling outer surface in the region of the heat source impact on it, i.e. at $0 < z < Z$, we assume

$$\lambda_3 \frac{\partial T_3}{\partial r}\Big|_{r = R_2 + \delta_2} = q_0, \qquad (11)$$

where q_0 is the density of the heat flow introduced through the coupling surface. For the remaining part of the coupling external surface, similar to (9), let us assume conditions of radiation heat exchange with the environment. As regards the inner boundary of region D_3, conditions of ideal thermal contact with the braze alloy layer are assigned that are satisfied at $z < L/2$ up to the moment of complete melting of the braze alloy initial layer and at $z < L'/2$ after change of the shape of region D_4, whereas at $L'/2 < z < L/2$ conditions of radiation heat exchange between the coupling inner surface and the piping surface are assumed.

Let us define the boundary conditions for the region occupied by the braze alloy (region *4* (*4′*) in Figure 1). On the boundary of this region, contacting the coupling metal, let us assign the conditions for the ideal thermal contact. On the inner boundary up to the moment of complete melting of the braze alloy, let us assume the conditions of radiation heat exchange with the piping surface that are replaced by the conditions of an ideal thermal contact after complete melting of the braze alloy. Finally, on the upper boundary of the considered region, i.e. at $z = L/2$ ($z = L'/2$ after the braze alloy melting), conditions of radiation exchange with the environment, are assigned.

This completes the definition of boundary problems for the equations of heat conductivity (1) for the case of the method of piping repair in space, considered in this paper. Note that the described model of thermal processes in brazing of the piping is a two-dimensional one unlike, for instance, the model suggested in [3], where unidimensional equations of heat conductivity were used for calculation of the temperature fields in brazing of thin-walled tubular items.

Modelling results. Equations (1) with the respective initial and boundary conditions were solved numerically by the finite difference methods. The derived differential equations were solved by the method of changing directions [4]. All calculations were made with the following geometrical parameters of the joint: $R_1 = 6$ mm; $\delta_1 = 1$ mm; $L = 20$ mm; $R_2 = 6.5 - 6.7$ mm. In this case thickness Δ of the braze alloy initial layer was varied in the range from 0.3 up to 0.5 mm so that the gap width between the coupling and the piping surface remained constant, equal to 0.2 mm*; $\delta_2 = 1 - 2$ mm. The piping and insert were of 10Kh18N9T (AISI 304) stainless steel; the coupling was of copper or the same steel. Considered as the braze alloy was Sn–Ni–Ge system alloy proposed in [5] with a high content of tin and, hence, close to tin values of thermophysical properties. All the required thermophysical properties of the above materials were taken from [6 – 8]. Temperature of stainless steel

* The above size of the gap is the maximal admissible one for brazing and it was selected allowing for the ability to perform manual assembly of the brazed joint during extravehicular activity.

brazing with the above braze alloy was assumed to be equal to 900 K.

First the optimal length of the zone of the coupling heating by the external heat source (heater) was determined. It was assumed that the heat flow was uniformly distributed over the external surface of the coupling within the region of $-Z < z < Z$ (see Figure 1), and its density q_0 was given by the following relationship:

$$q_0 = \frac{P}{4\pi(R_2 + \delta_2)Z}, \qquad (12)$$

where P is the total power applied to the item by the heater.

Modelling results demonstrated that the temperature fields that are the most optimal for brazing the considered joint, in the zone of the braze alloy contact with the piping surface, are in place when condition $Z_1 \approx L'/2$ is satisfied. Shortening of the heating area length is accompanied by overheating of the central regions of the coupling surface (up to melting of its material). Increase of Z_1 results in that after the braze alloy melting and formation of an ideal thermal contact between the coupling and piping in $z < L'/2$ region, the coupling outer edges are overheated. As a result, the temperature profile in the zone of the braze alloy contact with the surface of the piping and the insert is rising towards the coupling edges, this being especially significant in the case when a stainless steel coupling is used, which has a much lower heat conductivity than copper. Such a temperature profile in the brazing zone is inadmissible, as decrease of the contact angle of wetting of the surface being processed with the braze alloy, can lead to the braze alloy spreading to the coupling edges with the increase of this surface temperature, this, in its turn, not allowing a sound brazed joint to be made.

With the selected length of the heating zone (for the considered geometrical parameters of the joint, values $Z_1 = L'/2$ are in the range of 6.2 – 7.5 mm), calculations were performed of the dependence of temperature in different points of the item on the duration of its heating at the initial temperature T_a = 300 K (brazing in living compartments of the space vehicle). Figure 2 gives the appropriate dependencies for the central points of the piping external surface ($r = R_1$, $z = 0$) and central points of the coupling inner surface ($r = R_2$, $z = 0$). As follows from the presented curves, the piping surface temperature remains practically constant, equal to the item initial temperature, up to complete melting of the braze alloy, change of its shape under the impact of the surface tension forces and formation of an ideal thermal contact between the braze alloy and the piping surface. The temperature of the coupling inner surface, equal to the braze alloy temperature in appropriate points, at the initial stage of heating grows practically linearly in time (except for the process of braze alloy melting). Then, after contact of the molten braze alloy with the relatively cold surface, it is abruptly cooled down, while

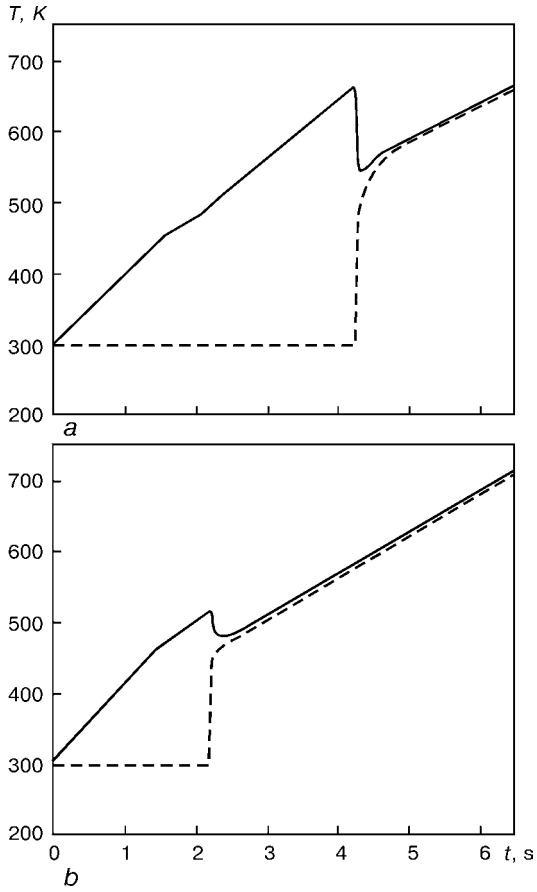

Figure 2. Dependence of temperature T in different points of the item on heating time t when a coupling of stainless steel 10Kh18N9T (a) and copper (b) is used at R_1 = 6.0 mm; δ_1 = 1.0 mm; R_2 = = 6.6 mm; δ_2 = 1.5 mm; Δ = 0.4 mm; P = 500 W; solid curves — for a point with co-ordinates $r = R_2$, $z = 0$; dashed curves — $r = R_1$, $z = 0$

the piping surface is heated so that their temperatures are equalised and further heating of the item leads to a linear growth of temperature in the brazing zone. Note that in the case when a copper coupling is used, complete melting of the braze alloy takes place almost 2 times faster than in the case of a stainless steel coupling (Figure 2), this being attributable to a higher heat conductivity of copper and its lower heat capacity.

As was already noted, contact of the molten braze alloy with the cold surface of the piping and the insert leads to considerable cooling down of the braze alloy (up to partial solidification) that is followed by further heating and fusion. Figure 3 shows the evolution of the thermal condition of the braze alloy after its contact with the piping surface; time was counted since the moment the braze alloy touched the surface being brazed.

In order to determine the energy characteristics of the brazing process, calculation was performed of the time of the joint heating up to the specified thermal condition and of the energy required for it, depending on the power applied to the item. The appropriate calculation data derived for the stainless steel coupling, are given in Figure 4, and for the copper coupling — in Figure 5. The lower curves in Figure 4, a and Figure 5, a correspond to the time of the joint

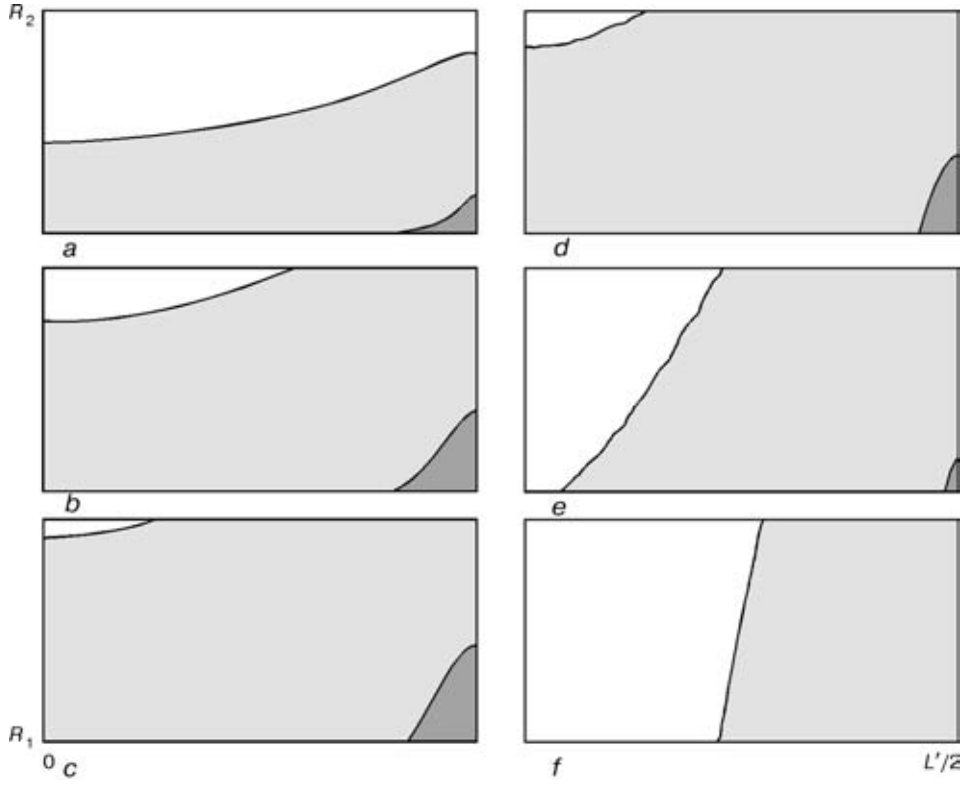

Figure 3. Evolution of the thermal condition of the braze alloy after its contact with the piping surface when a stainless steel coupling is used under the conditions, mentioned in Figure 2 and P = 250 W: unhatched areas correspond to the liquid condition of the braze alloy ($T \geq T_L$ = 493 K); dark areas — to the solid state ($T \leq T_S$ = 456 K); grey areas — to the intermediate state: *a* — t = 0.01; *b* — 0.04; *c* — 0.10; *d* — 0.20; *e* — 0.30; *f* — 0.40 s

heating up to complete melting of the braze alloy and establishment of an ideal thermal contact between the braze alloy and the piping surface. The lower boundary of the grey area corresponds to the time of achievement of the brazing temperature at least in one point of contact of the braze alloy with the piping surface, and the upper boundary — to the time of heating of the entire surface being brazed up to the specified temperature. Finally, the upper curves in these Figures correspond to the time of the start of melting of the coupling surface, i.e. limit the maximal admissible time of the item heating at the specified applied power.

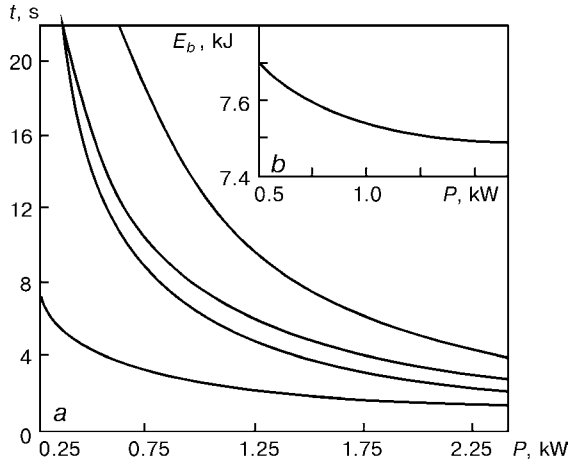

Figure 4. Dependence of time t of the item heating to the specified thermal condition (*a*) and energy E_b, required for the brazing process (*b*), on the input power P when a coupling of stainless steel 10Kh18N9T is used (R_1 = 6.0 mm; R_2 = 6.6 mm; δ_1 = 1.0 mm; δ_2 = 1.0 mm, Δ = 0.4 mm; T_a = 300 K)

As follows from the curves, given in Figures 4 and 5 the time of heating up to the specified thermal condition is naturally reduced with the increase of P. As regards the energy, required for heating the entire surface being brazed up to the brazing temperature, $E_b = Pt_b$, where t_b is the time of heating to the brazing temperature (upper boundary of the grey area in Figure 4, *a* and Figure 5, *a*), it is also reduced with the increase of power applied to the item (Figure 4, *b* and Figure 5, *b*). The cause for that is reduction of the share of energy losses for heat conductivity and radiation in the total energy balance of the joint under consideration with the increase of the speed of energy application, determined by value P.

Calculations showed that at other conditions being equal, the brazing time t_b, and, therefore, also energy E_b required for making the brazed joint, increase with the coupling wall thickness, practically in proportion to the increase of its material volume. In addition, the energy, required to provide the brazing process in the case a copper coupling is used, turns out to be approximately 20 % smaller than when a steel coupling is used (Figure 4, *b* and Figure 5, *b*). Thus, the method of making the brazed joint, that is the most energy effective in repair of stainless steel piping, is the use of a copper coupling of a minimal admissible thickness.

The optimal range of powers applied to the item by the heater, that are required for making the brazed

joint according to the schematic under consideration, is between 250 and 500 W, this amounting to not more than 1 kW of the consumed electric power, allowing for the efficiency of the heater proper and the process of heat transfer to the item. Such power levels, on the one hand, can be easily provided by the onboard power supply system of the space vehicle, and, on the other hand, allow brazing to be performed in a relatively short time (about 10 – 30 s). So, for instance, the time required to achieve the brazing temperature in all the points of the surface being brazed at P = 500 W, and T_a = 300 K, is equal to 12.3 s in the case of a copper coupling (Figure 4, *a*) and 15.5 s, if the coupling is of 10Kh18N9T (Figure 5, *a*). In addition, as follows from the same plots, applying such power to the item provides a sufficient (more than 6 s) time interval between the completion of the brazing process and the start of the coupling material melting.

Finally, if brazing is performed in raw space, the time for the joint heating up to the brazing temperature and the energy required for it, respectively, can essentially depend on the initial temperature of the item. In particular, in repair of piping on the sunlit side of the space vehicle, where the initial temperature is 400 K, the time of brazing the considered joint when a copper coupling is used, is 10.4 s (E_b = 5.2 kJ), whereas on the shadow side at T_a = 180 K — 14.4 s (E_b = 7.2 kJ).

In conclusion it should be noted that this work is of a theoretical nature and its results require experimental verification, including flight testing.

CONCLUSIONS

1. A mathematical model of thermal processes in brazing of piping in space, an appropriate computational algorithm and software for implementation of this model in the computer have been developed.

2. Modelling results have shown that use of a copper coupling in brazing of the considered joint, provides an energy saving up to 20 %, compared to the steel coupling, as well as allows achieving a more uniform distribution of temperature in the brazing zone.

3. In brazing joints of such geometrical dimensions, the most optimal powers are 250 – 500 W, applied to the item by the heater, thus allowing the zone of braze alloy contact with the piping surface to be heated up to the brazing temperature in 10 – 30 s.

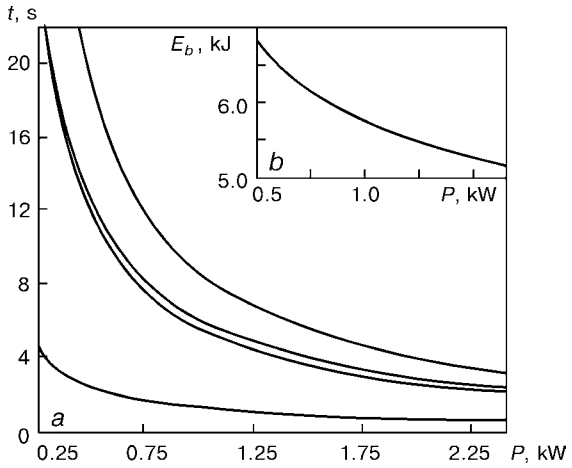

Figure 5. Dependence of the time of the item heating up to the specified thermal condition (*a*) and energy required for the brazing process (*b*) on the input power when a copper coupling is used (see parameters and designations in Figure 4)

REFERENCES

1. (2000) *Space: technologies, materials science, structures*. Ed. by B.E. Paton. Kyiv: PWI.
2. Kutateladze, S.S. (1979) *Fundamentals of heat exchange theory*. Moscow: Atomizdat.
3. Zelnichenko, A.T., Vakulenko, S.A., Bulatsev, A.R. *et al.* (1988) Calculation of heating of a multi-layer tubular item for brazing. *Avtomaticheskaya Svarka*, **2**, 30 – 32.
4. Anderson, D., Tannekhil, J., Pletcher, R. (1990) *Computational hydromechanics and heat exchange*. Moscow: Mir.
5. Zagrebelny, A.A., Gavrish, S.S., Bulatsev, A.R. *et al.* (1968) Analysis of permanent joints of tubular elements of braze-welding and brazing type made with URI. In: *Problems of space technology of metals*. Kyiv: PWI.
6. (1984) *Reference book on brazing*. Ed. by I.E. Petrunin. Moscow: Mashinostroyeniye.
7. Larikov, L.N., Yurchenko, Yu.F. (1985) Structure and properties of metals and alloys. In: *Thermal properties of metals and alloys*. Refer. Book. Kyiv: Naukova Dumka.
8. (1976) *Tables of physical values*. Refer. Book. Ed. by I.K. Kikoin. Moscow: Atomizdat.

EFFECTIVENESS IN USE OF MOLTEN POOL HEAT

V.V. DMITRIK and **V.V. SHEVCHENKO**
Ukrainian Engineering-Pedagogical Academy, Kharkov, Ukraine

ABSTRACT

Method for estimation of the amount of the arc heat introduced into parent metal and transferred with the liquid metal flows from the head to the tail portion of the weld pool is suggested. It is shown that the efficiency in use of the molten pool heat can be increased by using an extra filler metal and selecting the optimum parameters of welding.

Key words: *arc welding, arc heat, welding pool, overheating, heat consumption*

It is known that the arc heat introduced into the parent metal is consumed partially for the additional overheating the molten pool and HAZ metal [1 – 3]. First in welding of thin-walled structures the displacement of height of penetration of edges from the region of the arc spot to the side of the pool tail portion was observed by A.I. Akulov in his thesis for the degree of Dr. of Technical Sciences. Many works were devoted to the study of processes proceeding in the molten pool [4 – 6, etc.]. The quantitative estimation of degree of overheating the pool melt was carried out by us during calculations of the temperature conditions [7 – 9]. To improve the structure of mathematical models of heat problems, realized by numerical methods, and to optimize the parameters of welding conditions it is rational to determine the amount of arc heat which is transferred by the molten metal flows from the head to tail portion of the pool.

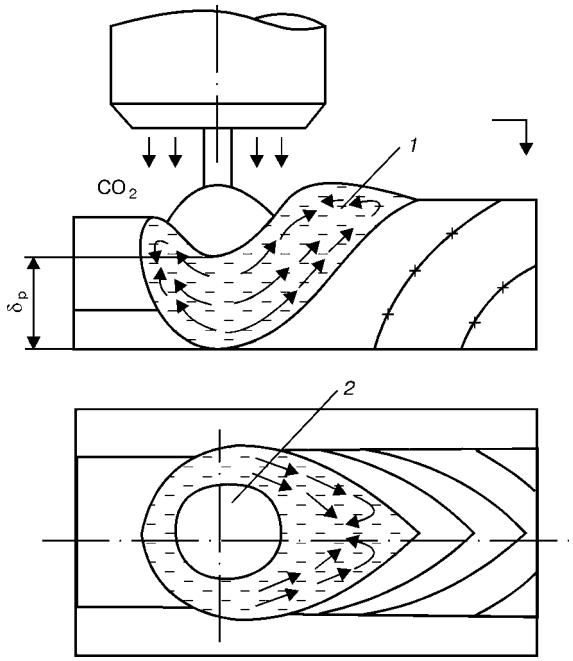

Figure 1. Diagram of movement of molten metal flows from head to tail portions of the weld pool: *1* — pool melt; *2* — region of arc active spot (δ_p — molten pool depth)

Therefore, it is important to determine the auxiliary overheating in welding steels, prone to the formation of hardened structures, including pearlitic steels which are widely used in power engineering. It is also rational to determine the coordinates of overheated regions, at which the structures, not meeting the requirements of standard documentation, are formed. It was established that the volume of overheated regions with similar structures in welded joints can be different. Such structures are observed also in local volume regions. In structure of weld metal (bainite + ferrite, steel 08KhMF (C — 0.8; Cr — 1.0; Mo — 1.0; V — 1.0 wt.%; Fe — balance)) these may be enlarged matrix grains α-Fe, which are characteristic of a high degree of phase stresses. The additional heating can also promote the formation of «soft» ferritic or «hard» martensitic interlayers at the region of HAZ metal fusion. So, the overheated region should not be admitted, if possible, to form the optimum initial structure.

The presence of overheated regions is not also desirable during the weld formation [5] as they increase the degree of residual stresses and strains.

It was established [6, 7, 9] that during the automatic welding at medium conditions (I_w = 280 – 380 A; v_w = 20 – 25 m/h; U_a = 28 – 32 V; electrode wire diameter — 2 mm) the main flow of molten metal from the head to tail portion of the pool is spread in the melt region adjacent to the crystallization surface (Figure 1). In accordance with the presented diagram of the flow the current-free auxiliary filler wire (AFW) was injected to the weld pool (Figure 2). The rate of AFW injection was 50 – 60 m/h, and the frequency of this wire movement in the melt region adjacent to the crystallization surface was 50 – 60 movements per minute.

Let us consider that the amount of heat transferred by the molten metal flows from head to tail part of the pool corresponds to the amount of heat consumed for the AFW melting. The mentioned process will be considered as quasi-steady with a constant rate of AFW injection to the molten pool. It is also assumed that the AFW, injected to the pool, has a form of a semi-finite bar (Figure 2). Error at absence of allowance for a latent heat of melting does not exceed 10 % of the heat amount consumed for AFW melting at the region *1* (Figure 2). The allowance for the latent heat

Width (averaged) of regions of HAZ metal of samples* of 60 mm thickness, welded at conventional and suggested conditions

Automatic welding conditions	*HAZ region, mm*			
	fusion	*overheating*	*normalizing*	*partial recrystallization*
Suggested	0.1 – 0.2	0.6 – 0.7	2.0 – 3.0	1.2 – 1.4
Conventional	0.2 – 0.3	0.7 – 0.8	2.5 – 3.5	1.4 – 1.7

*Samples were made of steel 15Kh1M1 (C — 0.15; Cr — 1.0; Mo — 1.0 wt.%; Fe — balance); electrode wire Sv-08KhMF; tempering at 730 °C, 3 h.

can be made by introducing correction coefficients k, determined experimentally: $k_1 = 1.1$ at the region *1*, $k_2 = 1.07$ at the region *2*. The amount of the molten pool heat, consumed for AFW melting (Figure 2) taking into account the known statements [10] and averaged values $c_i(T)$, $\gamma_i(T)(i = 1, 2, 3)$, whose data were taken from [3], will be written

$$Q = k_1 S_{l_{av}} c_1 \gamma_1 \frac{T_0 - T_1}{2} l_1 + \\ + k_2 S_0 c_2 \gamma_2 \frac{T_1 - T_2}{2} l_2 + S_0 c_3 \gamma_3 \frac{T_2 - T_3}{2} l_3, \quad (1)$$

where S_0 is the AFW section at region from l_1 to $+\infty$, mm^2; $0–l_1$ is the length of region of AFW melting, mm; $l_1–l_2$ is the length of region of AFW, located in pool, mm; $l_2–l_3$ is the length of region of AFW, in which it is preheated from the side of molten pool, mm; γ is the density at the i-th region of AFW, kg/m^3; c is the heat content (mass) at the i-th region of AFW, J/(kg·°C); α is the angle (Figure 2) determined experimentally; $T_0 = (1770 \pm 50)$ °C is the averaged temperature at the region of AFW melting; $T_1 = 1770$ °C — $(1770 - 1500)$ °C/2 = (1650 ± 50) °C is the mean value of temperature at the region of contact $l_1–l_2$ of AFW, injected to the pool with a melt; $T_2 = 1500$ °C is the temperature at the surface of the molten pool; $T_3 = 20$ °C is the environmental temperature; $S_{l_{av}}$ is the averaged area of cross section of a cone-shaped region of AFW melting, mm^2,

$$S_{l_{av}} = \pi r^2_{l_{av}} = \frac{\pi l_{av} \mathrm{tg}^2 \alpha}{4};$$

$r_{l_{av}}$ is the averaged radius of cone base of region of AFW melting, mm.

It was determined that the heat consumption for the AFW melting and heating in welding using the mentioned conditions is 7 – 10 % from the arc heat introduced into the parent metal. It can be considered that the heat, close to the quantitative characteristic, is transferred by the molten metal flows from head to tail portion of the weld pool.

It is known that the use of an auxiliary filler metal in the mechanized welding can decrease the overheating of the pool melt and HAZ metal. The application of the mentioned processes of welding can be promising [11], including, in the opinion of V.N. Zemzin [12], for welding of pearlitic steels.

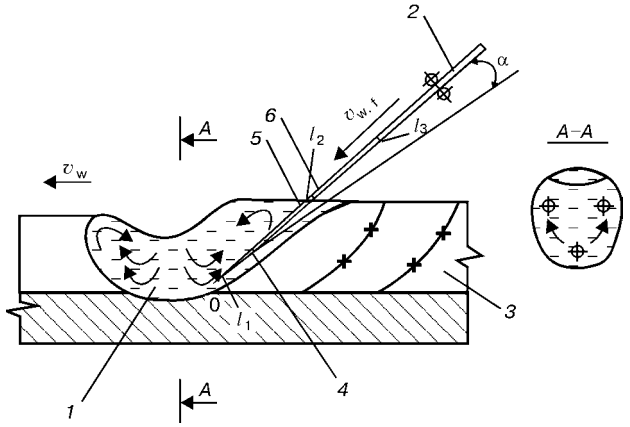

Figure 2. Diagram of AFW feeding to the pool tail portion in accordance with diagram of Figure 1: *1* — molten pool; *2* — AFW; *3* — weld metal; *4* — region of $0–l_1$ length for AFW melting; *5* — region of $l_1–l_2$ length for melting of AFW located in molten pool; *6* — region of $l_2–l_3$ length for AFW melting, subjected to preheating by a pool heat; $v_{w.f}$ — speed of AFW feeding in the apex of forming cone at its melting

The decrease in overheating can also be reached in welding at the conditions whose parameters are based on the results of modelling the processes of heat exchange and crystallization in the region of molten pool, metal of weld and HAZ [13]. This was proved by obtained experimental sizes of regions of HAZ metal of welded joints made by the automatic welding in CO_2 at conventional and suggested (based on modelling results) conditions (Table).

During welding at the suggested condition the penetration of parent metal edges and also of metal of the previous layers was sufficient. Moreover, there were no defects of «lack of fusion» type in gap walls and between the beads.

The presence of normalizing regions of larger sizes than that of the overheating region was observed in separate welded joints made from low-alloyed pearlitic Cr–Mo–V steels. In our opinion, the process of formation of structures of these regions requires separate study, taking into account the peculiarities of heat distribution.

The realization of the suggested method of calculated-experimental determination of amount of heat

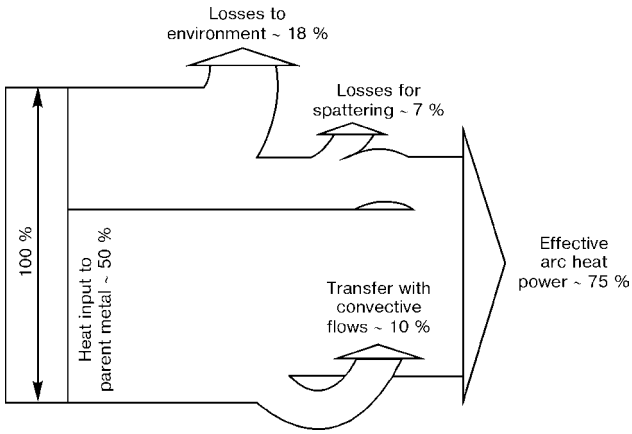

Figure 3. Diagram of heat balance of the automatic welding in CO_2

transferred by the molten metal flows from the head to tail portions of the pool made it possible to correct the known diagram of heat balance of the welding process (Figure 3).

With the use of estimated data it seems possible to develop the methods of welding which will decrease the overheating of the molten pool and HAZ regions and promote the producing of welded joints with an optimum initial structure, including that of pearlitic steels.

REFERENCES

1. (1974) *Technology of electric welding of metals and alloys by fusion*. Ed. by B.E. Paton. Moscow: Mashinostroyeniye.
2. Akulov, A.I., Belchuk, G.A., Demyantsevich, V.P. (1977) *Technology and equipment for fusion welding*. Moscow: Mashinostroyeniye.
3. (1967) *Physical properties of steels and alloys used in power engineering*. Handbook. Ed. by B.E. Nejmark. Leningrad: Energia.
4. Vopopaj, N.M., Kornienko, A.N., Kostenyuk, N.I. *et al*. *Method of measuring the force action of arc on weld pool in consumable electrode welding*. USSR author's certificate **1727972**, Int. Cl. B 23 K 31/12. Publ. 23.04.92.
5. Akulov, A.I., Chernyshov, G.G., Doronin, Yu.V. *et al*. (1978) Effect of hydrodynamic phenomena in weld pool on the formation of butt welds in consumable electrode welding. *Izvestiya Vuzov, Mashinostroyeniye*, **6**, 135 – 139.
6. Akulov, A.I., Dmitrik, V.V., Babushkina, V.A. *Method of determination of direction of movement of molten metal flows from head to tail portion of weld pool*. USSR author's certificate **1176524**, Int. Cl. B 23 K 31/12. Publ. 23.11.92.
7. Dmitrik, V.V. (1998) Method of determination of temperature condition in molten welding pool. *Svarochnoye Proizvodstvo*, **8**, 19 – 21.
8. Dmitrik, V.V. (1999) Development of method of determination of temperature condition of molten pool. *Izvestiya Vuzov, Mashinostroyeniye*, **1**, 76 – 80.
9. Dmitrik, V.V. (1990) Estimation of arc heat introduced to parent metal. *Ibid*., **4**, 119 – 122.
10. (1988) *Theory of welding processes*. Ed. by V.V. Frolov. Moscow: Visshaya Shkola.
11. Kasatkin, B.S., Volkov, V.G. (1977) Application of cut wire as a filler material in automatic welding of high-strength steels. *Avtomaticheskaya Svarka*, **7**, 41 – 45.
12. Zemzin, V.N. (1972) *Heat resistance of welded joints*. Leningrad: Mashinostroyeniye.
13. Dmitrik, V.V. (1999) Stabilization of conditions of automatic welding of pearlitic steels. *Svarochnoye Proizvodstvo*, **5**, 11 – 14.

ABOUT THE FORM OF HYDROGEN EXISTENCE IN WELDING FUSED FLUXES

I.A. GONCHAROV[1], A.P. PALTSEVICH[1], V.S. TOKAREV[1], T.S. VEBLAYA[2] and N.P. KHARCHENKO[2]
[1]The E.O. Paton Electric Welding Institute, NASU, Kyiv, Ukraine
[2]Taras Shevchenko Kyiv National University, Kyiv, Ukraine

ABSTRACT

The forms of hydrogen existence in welding fused flux AN-348A were examined using the methods of IR-spectroscopy, thermogravimetry and gas chromatography. As model substances the zeolite NaA and kaolin were used. A significant difference of flux AN-348A from the zeolite is shown by a nature of a thermal hydrogen desorption. It is established that the main part of the latter is dissolved in the flux examined during the process of furnace melting in the form of a hydroxyl and removed at heating above 800 °C.

Key words: *hydrogen, water, hydroxyl, fused flux, zeolite, kaolin, thermal desorption*

Hydrogen is the cause of formation of pores in welds during SAW and also of cold cracks in welded joints made from the low-alloyed high-strength steels. The welding flux is one of the main sources of hydrogen [1]. At the same time the quality welds can be provided by using the welding consumables containing the diffusive hydrogen in the deposited metal of not more than 5 $cm^3/100$ g of metal [2]. For this purpose, it is necessary to investigate both the content of a potential hydrogen and also the forms of its existence in welding fluxes. The available data are limited. Thus, in work of Yu.D. Brusnitsyn [3] the water removal from fluxes was studied by heating and measurement of losses in mass of sample of fluxes 48-OF-6 and 48-OF-10 of slag systems CaF_2–Al_2O_3–CaO and CaF_2–Al_2O_3–MgO–SiO_2, respectively, which are susceptible to the formation of crystalline structures. The conclusion was made on the basis of mode of water removal about the dominating presence of a zeolite water in fluxes which is adsorbed during their manufacture at the stage of a wet granulation independently of structure of grains (pumice-, stone-, glass-type) and removed within the temperature range of 200 – 1100 °C. In [4, 5] this conclusion is valid for all the fluxes, including the acid slag systems MnO–SiO_2–CaF_2.

However, according to data [6], the water, adsorbed in structural voids, is almost completely removed in heating of natural and synthetic zeolites up to the temperature of order of 400 °C. At the same time, according to data of I.A. Novokhatsky [7], the removal of dissolved water during heating from metallurgical slags in which it is present in the form of hydroxyl groups OH^-, is started from 750 °C and higher. It is also known [6] that hydrogen contained in alumosilicates in the form of hydroxyl anions OH^- is removed during heating in the form of water whose temperature of desorption can reach more than 900 °C depending on the bond of anions OH^- with cations of the alumosilicates.

Model of water existence in minerals, used by Yu.D. Brusnitsyn [3], does not take into account the slag contact with a water vapour during its melting in furnace. In the more recent work [8] the same author recognizes the feasibility of its dissolution in the slag melt during melting when he explained the presence of water in the flux of a dry granulation. In his opinion [8] the determination of water content by losses in mass of the sample, which was used by him in [3], cannot provide the reliable results because large errors can be made by the formation of volatile fluoride compounds and oxidation of separate components.

In works [9, 10] the authors came to the conclusion that a large amount of hydrogen is available in the fused fluxes in the form of hydroxyl OH^-. However, the technology of manufacture and composition of fluxes were not mentioned there. In addition, in [9] the latter were investigated after calcination at 600 °C that does not give information about the complete content of hydrogen in them.

To clarify the forms of existence and content of hydrogen in the fused fluxes, the flux AN-348A and also kaolin and synthetic zeolite NaA (as model substances, contained water in different forms) were investigated. The flux AN-348A, which belongs to the slag system MnO–SiO_2–CaF_2, has a dense glass-type structure of the grains which have no inner cavities. The synthetic zeolite NaA consists of alternating tetrahedrons SiO_4 and AlO_4, joined with each other by apexes. Zeolite NaA has a frame with a ratio Si/Al = = 1 and cavities of about 0.4 nm diameter. Water molecules, filling these voids, are connected to this frame by the adsorption forces. In kaolin the hydrogen exists in its structure in the form of OH-groups [6].

The forms of hydrogen existence were examined by the method of IR-spectroscopy using spectrophotometer Specord M-80. Samples were prepared in the form of suspension of crushed grains of the substance in a purified vaseline oil and deposited on the potassium bromide. The thermal desorption of water from the substances was made by the methods of a thermogravimetric analysis and gas chromatography [11].

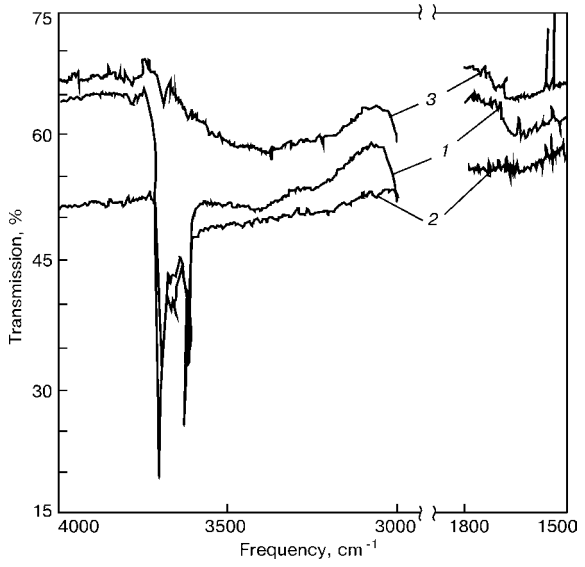

Figure 1. IR-spectrum of transmission of kaolin sample in initial state (*1*), calcinated at 170 °C for 4 h (*2*), as well as at 650 °C for 2 h and holding in air (*3*)

O–H bonds of molecular water and hydroxyl are characteristic of appearance of different typical bands of absorption during passing of IR-beams through the substance. This is associated with exciting of valence and deformation vibrations of atoms (movements of atoms, respectively, along the valence bond and with a change in angle between two bonds).

In the region of valence vibrations of OH-groups the IR-spectrum of the kaolin sample (Figure 1) has narrow intensive bands of transmission of free hydroxyl groups (not bound with hydrogen bonds with other hydroxyls or water molecules) at the frequency of 3620 and 3696 cm^{-1} and wide lower-intensive band of transmission within the range of 3072 – 3575 cm^{-1} frequencies. The latter corresponds to the valence vibrations of OH-groups of the molecular water adsorbed on the kaolin surface. In the IR-spectrum of kaolin, calcinated at 170 °C for 4 h, this band disappears. In addition, there are no bands of transmission in the region of deformation vibrations of OH-groups (1500 – 1700 cm^{-1}), typical only of the molecular water, that was informed in [12]. After kaolin calcination for 2 h at 650 °C and its soaking in air, there were no narrow intensive bands of valence vibrations of free hydroxyl groups in the IR-spectrum, included earlier into the kaolin structure. After its further air soaking these bands are not recovered, only slight wide bands appear which correspond to valence and deformation vibrations of the adsorbed water.

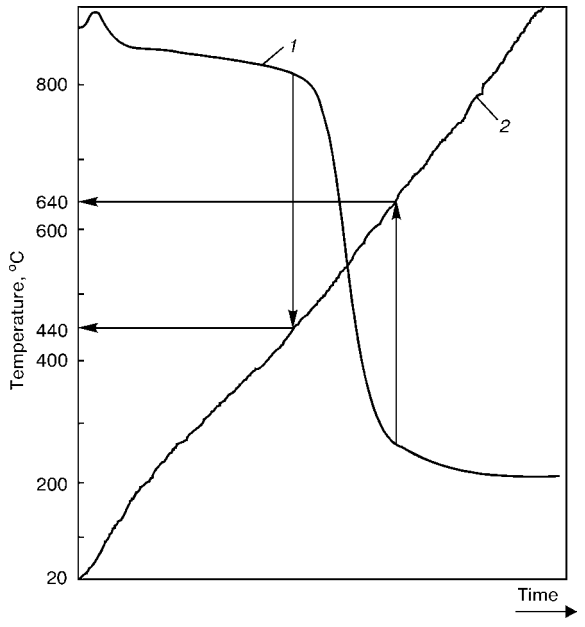

Figure 2. Derivatogram of kaolin sample: *1* — curve of mass losses; *2* — curve of heating

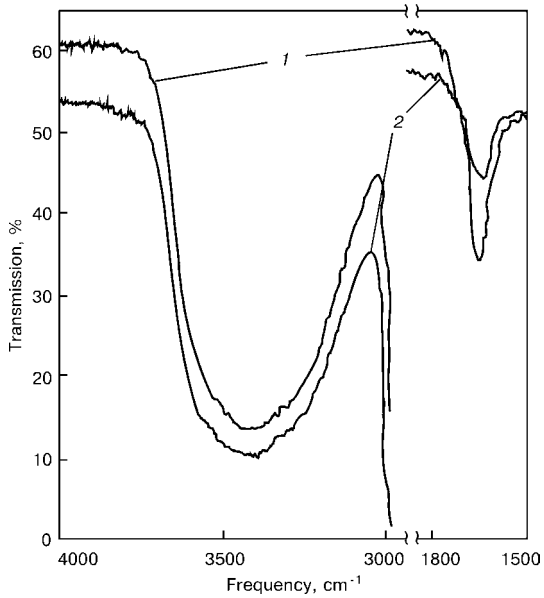

Figure 3. IR-spectrum of transmission of zeolite NaA sample calcinated at 170 °C for 4 h (*1*) and with a subsequent holding in air for 14 days (*2*)

Thermogravimetric analysis of the kaolin sample was made using a derivatograph Q-1500D. It was established that within the 440 – 640 °C interval (Figure 2) the loss in mass (about 14 %) occurs due to water liberation. These results have a good correlation with those obtained in [11] where it was shown, using the gas chromatography method, that the hydrogen existing in kaolin in the form of hydroxyl is evolved in the form of water at 550 – 620 °C temperature.

Sample of zeolite NaA was dried during 4 h at 170 °C and then its spectrum of transmission was examined after cooling (Figure 3). It has an intensive wide band of 3040 – 3584 cm^{-1} frequencies with maximum at 3384 cm^{-1} in the region of valence vibrations of OH-groups. In the region of deformation vibrations of OH-groups one more wide band in the range of 1500 – 1800 cm^{-1} frequencies with maximum at 1652 cm^{-1} is observed. The mentioned bands correspond to the hydrogen bond of hydrogen of water molecules with ions of oxygen from the zeolite frame. This is explained by an intensive adsorption of water from the air by the sample surface during cooling before the analysis. The next zeolite holding in air during 14 days does not lead to increasing the intensity of bands in the region of valence and deformation vibrations. This proves that hydration of water by zeolite from the air is most intensive at the first minutes of its contact with atmospheric moisture and then

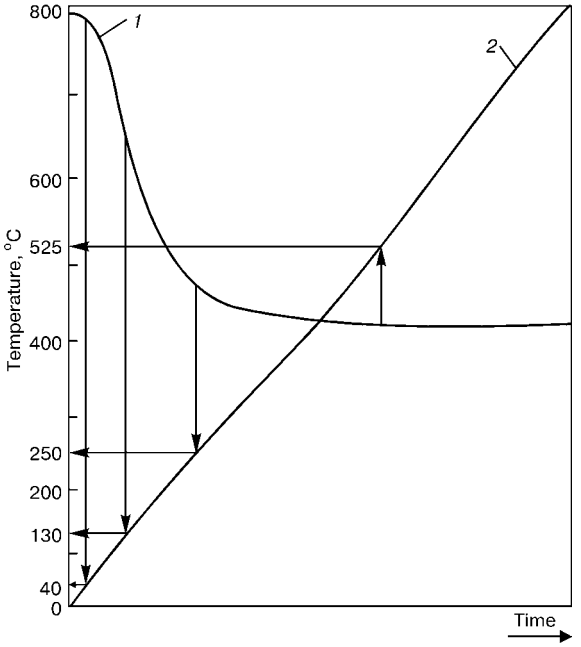

Figure 4. Derivatogram of zeolite NaA sample: *1* — curve of mass losses; *2* — curve of heating

it is reduced on filling the frame voids with water molecules.

According to the derivatogram of zeolite NaA (Figure 4) the loss of its mass at the expense of thermal desorption of water molecules from the sample starts at the temperature of about 40 °C, reaches maximum at 130 °C, reduces a little at 250 °C, and then it is interrupted completely at 525 °C. The total loss of mass by the zeolite (relative humidity) is 32.4 %.

The chromatogram of the water thermodesorption from zeolite NaA during heating at the 12 – 14 °C/min rate is given in Figure 5. It is characterized by the presence of maximum at 190 °C temperature and finishing of the process of water liberation at 535 °C. This non-equilibrium heating caused, probably, the formation of a small amount of desorbing water at 680 °C. The temperature mode of water desorption is coincided with data obtained by the method of a thermogravimetric analysis (Figure 4). Moreover, the total hydrogen content in the zeolite sample is 22200 cm^3/100 g.

IR-spectrum of flux AN-348A (Figure 6) differs greatly from those which were described earlier for kaolin and zeolite. It contains a slight blurring band of transmission of valence vibrations of OH-groups within the interval of frequencies 3100 – 3700 cm^{-1}. In IR-spectrum of the flux calcinated at 800 °C for 2 h, this band is somewhat decreased, but not disappeared completely. Probably, it is due to the contact of the calcinated flux with an atmospheric moisture of the air during preparation of the sample for the analysis (water adsorption at its surface occurs).

The spectral region of frequencies 3100 – 3700 cm^{-1} is characterized by the valence vibrations of OH-groups corresponding both to water, adsorbed by the surface and capillaries, and also to hydroxyl groups, bound with the structure of the substance of a different degree of strength. The separate identification of forms of hydrogen in the fused fluxes having significantly lower its mass contents (less than 0.1 %) as compared with zeolite and kaolin, is difficult. It is noted in [12] that in the region of the valence vibrations it is impossible to divide adequately the bands referring to valence vibrations of structural hydroxides and water molecules. In the region of 1500 – 1700 cm^{-1} frequencies of deformation vibrations of OH-groups typical only of molecular adsorption of H_2O on the IR-spectrum of flux AN-348A the transmission bands are present, but they are very weak. This flux was not examined by the method of thermogravimetry, because in the process of heating of manganese-silicate fluxes the loss in mass, due to a water liberation, is observed simultaneously with its increase, because of manganese oxidation and also losses caused by precipitation of the silicon tetrafluoride. The latter occurs as a result of interaction of silicon dioxide and calcium fluoride included into the flux composition.

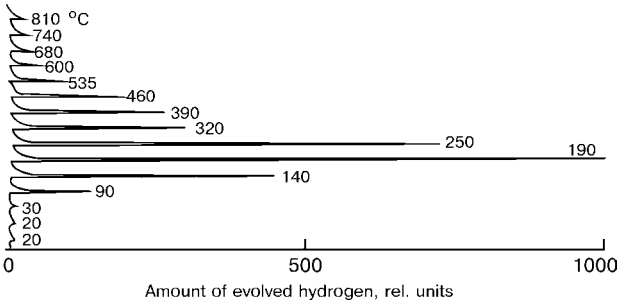

Figure 5. Chromatogram of thermal desorption of hydrogen from zeolite NaA sample

The important information about the forms of hydrogen in fused fluxes can be obtained by study of the kinetics of hydrogen evolution from fluxes during their heating using a method of a gas chromatography.

Figure 7 shows the chromatogram of thermal desorption of water from flux AN-348A. The nature of this process differs greatly from the thermodesorption of zeolite NaA (see Figures 4 and 5). The amount of hygroscopic moisture removed during heating to 200 °C is up to 5 % of its total mass content, while during heating to 600 °C it is about 15 %. At a further heating the amount of the removed water is increased. The first maximum at 790 °C temperature is coincided with an exothermic effect on the curve of a differential thermal analysis of flux AN-348A [13], caused by the growth of crystals. This results in a «jumpy» water liberation, thus explaining the presence of two peaks

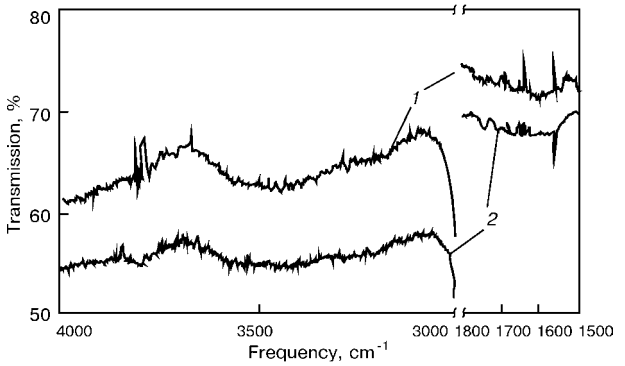

Figure 6. IR-spectrum of transmission of flux AN-348A: *1* — initial; *2* — after calcination at 800 °C for 2 h

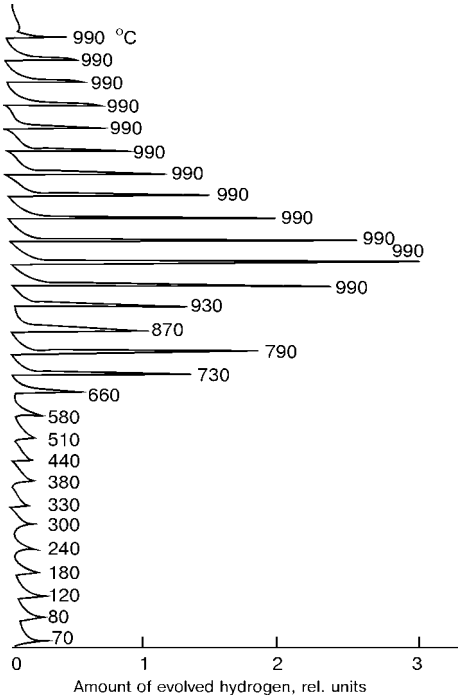

Figure 7. Chromatogram of thermal desorption of hydrogen from flux AN-348A

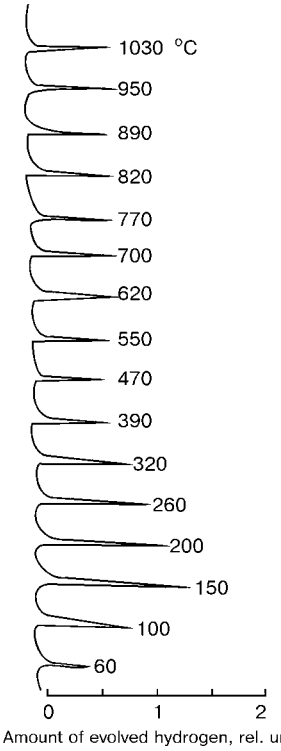

Figure 8. Chromatogram of thermal desorption of hydrogen from flux AN-348A, calcinated at 800 °C for 2 h

on the chromatogram. The main amount of water is liberated within the 930 – 990 °C temperature interval. The high-temperature mode of its liberation is observed in heating of white mica to 1000 °C in which hydrogen is in the form of a hydroxyl group OH^- [11]. The total hydrogen content in the examined sample of flux AN-348A was 32 $cm^3/100$ g.

To confirm the assumption about the fact that the water desorbed from the flux AN-348A is dissolved in it at high temperatures during the process of furnace melting in the form of OH-group, the Figure 8 presents the chromatogram of thermal desorption of hydrogen from the sample of flux AN-348A calcinated at 800 °C for 2 h and held in air during a month. It is seen in the chromatogram that after the calcination the flux sample has no high-temperature fraction of water which could dissolve in it during melting. Difference in values of temperatures of water desorption on the chromatograms (Figures 7 and 8) is, probably, caused by a non-equilibrium mode of heating during analysis as compared with calcination at 800 °C for 2 h and a low coefficient of diffusion of OH-group [7]. Hydrogen, whose content in the calcinated flux AN-348A was about 8 $cm^3/100$ g, had mainly the form of a moisture adsorbed at the flux surface during its holding after calcination.

CONCLUSIONS

1. Examination of the fused flux AN-348A, zeolite NaA and kaolin was performed using the methods of thermogravimetry, IR-spectroscopy and gas chromatography.

2. Welding fused flux AN-348A is differed from zeolites by a total content and kinetics of thermal desorption of hydrogen. The existing conception about the dominating presence of a «zeolitic» water in the fused fluxes is erroneous.

3. There is a negligible amount of adsorbed water at the surface of grains of glass-type fused flux AN-348A. The main amount of hydrogen is evolved in the form of moisture during heating above 800 °C. It is most probable, that this is hydrogen which is dissolved in the flux during its furnace melting and available in the form of a hydroxyl OH-groups.

REFERENCES

1. Kirdo, I.V. (1950) About composition of gases surrounding the arc during submerged arc welding. *Avtomaticheskaya Svarka*, **1**, 50 – 59.
2. Pokhodnya, I.K., Paltsevich, A.P., Golovko, V.G. *et al.* (1998) Technological and metallurgical methods of decreasing the absorption of hydrogen in welding. In: *Coll. of papers of 1st Int. Conf. of CIS on Welding Consumables*, Krasnodar, June 22 – 26. Moscow: OAO «AO Spetselektrod».
3. Brusnitsyn, Yu.D. (1958) About hydration of welding fused fluxes. *Welding*, Issue 1. Leningrad: Sudostroyeniye.
4. Potapov, N.N. (1979) *Fundamentals of selection of fluxes in welding of steels*. Moscow: Mashinostroyeniye.
5. Kovach, Ya., Petrov, G.L. (1974) Investigation of hydration and dehydration of acid fluxes for the automatic arc welding of steels. In: *Welding fluxes and slags*. Kyiv: Naukova Dumka.
6. Betekhtin, A.G. (1950) *Mineralogy*. Moscow: Gosgeologizdat.
7. Novokhatsky, I.A. (1975) *Gases in oxide melts*. Moscow: Metallurgia.
8. Brusnitsyn, Yu.D., Vitol, E.I. (1963) About determination of water in welding fluxes. *Welding*, Issue 6. Leningrad: Sudpromgiz.
9. Frolov, Yu.V. (1981) Fused flux as a hydrogen source in welding. *Avtomaticheskaya Svarka*, **6**, 57 – 58.
10. Tsuboi, J., Terashima, H. (1973) The behavior of hydrogen in arc welding. *J. JWS*, **6**, 544 – 553.
11. Paltsevich, A.P. (1998.) Chromatographic method of hydrogen content determination in components of electrode coatings. In: *Coll. of papers of 1st Int. Conf. of CIS on Welding Consumables*, Krasnodar, June 22 – 26. Moscow: OAO «AO Spetselektrod».
12. Zarifiants, Yu.A., Kiselev, V.F., Khrustaleva, S.V. (1974) About infrared spectra of hydrate coating of oxides. In: *Bound water in dispersed systems*. Moscow: MSU.
13. Veblaya, T.S., Kharchenko, N.P., Shevchenko, L.A. *et al.* (1981) Effect of method of granulation on structure of welding flux. *Khim. Tekhnologiya*, **3**, 61 – 62.

OPTIMIZATION OF CHEMICAL COMPOSITION OF DEPOSITED METAL OF COMPONENTS OPERATING UNDER THE CONDITIONS OF ABRASIVE WEAR

S.N. POPOV
Zaporozhje State Technical University, Zaporozhje, Ukraine

ABSTRACT

Results of planning and processing of experimental data to optimize the chemical composition of the deposited metal possessing high wear resistance are presented. The effect of carbon, boron and vanadium in ferro-chromium (13 % Cr) alloys on their resistance to the abrasive wear is determined.

Key words: *deposited metal, wear resistance, chemical composition, regression*

It was stated earlier [1 – 3] that the use of standard surfacing materials does not always guarantee the high resistance to abrasive wear of components of road-construction equipment, since it does not take into consideration the definite service conditions. This refer, in particular, to the elements of working components of the asphalt mixers. An attempt was made in the present work to optimize the chemical composition, deposited with allowance for the conditions of wear. In accordance with [3, 4] the most promising materials for the components of the mixing equipment are the alloys of a high initial hardness (*HRC* 58 – 68) and large content (50 – 80 %) of a strengthening excessive phase, which is characterized by the following microhardness: *HV* 16 – 30 GPa. Materials having martensitic-austenitic matrix meet these conditions. We suppose that hypereutectic alloys of Fe–C–Cr–B–V system which do not contain scarce elements and are crystallized with a different excessive phase: carbide M_7C_3, $M_{23}C_6$; boride MB, M_2B; carboboride $M_{23}(CB)_6$, etc., depending on the ratio of chromium content to carbon and boron, are correlated sufficiently well with the specified requirements. The presence of a wide spectrum of forming hard inclusions defines the high potentialities of the given system of alloying, as it allows selection of those required optimum ratios of amount of different types of the strengthening phase which provide the maximum wear resistance of the metal under conditions of service of working elements of the road-construction machines. A relative linear wear resistance ε_L (reference — as-annealed steel 45 (C — 0.45 wt.%; Fe — balance)) was selected as a parameter of optimizing.

When planning the experiments, the content of alloying elements was selected as variables whose effect on the wear resistance of materials was studied in [5] and it was necessary to establish only their combined effect on the ability to wear resistance of metal under the given service conditions. The following factors were taken as basic and independent: mass share of carbon, boron and vanadium in the deposited metal. The mass share of the chromium remained constant and was equal to 13 %. This is associated with the fact that chromium introduction into the deposited metal was necessary for the formation of the chromium carbides, borides or carboborides. And chromium content in the alloy should be limited to 13 – 16 %, as the authors of [4, 5] found that the increase in chromium content above 15 – 20 % does not lead to the increase in wear resistance of the surfacing materials used under the conditions of intensive abrasive wear.

Experiments were performed according to the plan of type B_3 [6], containing the complete factorial experiment 2^3, centres of faces and cube. The content of alloying elements was varied within the following ranges, %: C — 1.0 – 2.5; B — 1.0 – 4.0; V — 0.5 – 3.0 at a mean content of 1.75 C, 2.5 B and 1.75 V.

Taking into account the investigations performed it was rationally to set the lower level of alloying with carbon and boron of not less than 1 %, as, here, the amount of the strengthening phase is decreased (less than 30 %), thus causing the unjustified factorial space in the region of alloys with the expected low wear resistance [3 – 5]. The limitations by an upper level of alloying with carbon and boron (2.5 and 4.0 %, respectively) are due to the feasibility to provide the calculated chemical composition of the metal produced by melting of the 3.0 mm diameter flux-cored wire.

The selection of intervals by vanadium varying was based on the fact that it is rational to set the lower level of not less than 0.5 % (due to not clear manifestation of effect of low content of vanadium on the alloy wear resistance) and the upper level should not exceed 3 % (at high contents the wear resistance of the metal base is deteriorated, being caused by depletion of the solid solution with carbon used for the formation of the vanadium carbides [5]).

It should be noted that the accepted selection of varying limits is approximate and allows determination only of the boundaries of changing the alloying

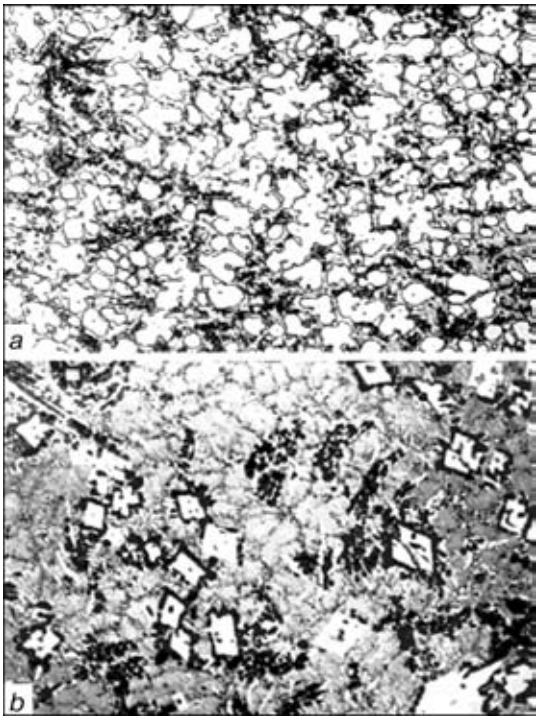

Figure 1. Microstructure of deposited metal with different relative wear resistance (in accordance with Table): *a* — 4.64; *b* — 6.24 (×300)

Matrix of planning

Mass share of elements, %			*Initial hardness, HRC*	*Microhardness, GPa*		*Linear relative wear resistance,* ε_L
C	*B*	*V*		*Base*	*Strengthening phase*	
1.00	1.0	3.00	58	10.36	–	4.64
1.00	4.0	0.50	65	7.12	22.81	9.04
2.50	1.0	0.50	62	9.41	–	5.67
2.50	4.0	3.00	65	8.28	19.56	5.23
1.00	1.0	0.50	56	6.91	–	4.19
1.00	4.0	3.00	64	7.34	21.76	8.64
2.50	1.0	3.00	63	12.60	–	7.82
2.50	4.0	0.50	65	7.69	18.52	6.12
1.75	2.5	1.75	62	5.05	15.14	6.24
1.75	4.0	1.75				9.57
1.00	2.5	1.75				8.58
2.50	2.5	1.75				9.21
1.75	2.5	0.50				9.24
1.75	2.5	3.00				6.90
2.50	2.9	1.60				8.84

elements as it does not take into account the number of peculiarities of formation of solid phases, as well as the effect of technological factors during surfacing. Thus, during the carbide formation a part of carbon is substituted for atoms of boron and other elements. The lattice of carbides is scarce in carbon that decreases the number of elements bound into carbides. At the same time it can determine the region of the factorial space, in which the alloy with a maximum wear resistance may locate at a preset system of alloying Fe–C–Cr–B–V. The results of experiments are given in Table .

Microstructure of the deposited metal of the examined materials by a matrix of planning with different relative wear resistance is given in Figure 1.

After processing of experimental data the regression dependencies of wear resistance on content of alloying elements were obtained, which are presented in Figure 2. Analysis of obtained relations shows that carbon, boron and vanadium enter the equation with sign «plus» and cause the increase in metal wear resistance, though their simultaneous effect may cause some reduction of the alloy to the abrasive wear resistance. The negative triple effect is due, probably, to «competitiveness» of carbon, boron, vanadium in increasing the wear resistance of metal, as during its crystallization the different processes are occurred,

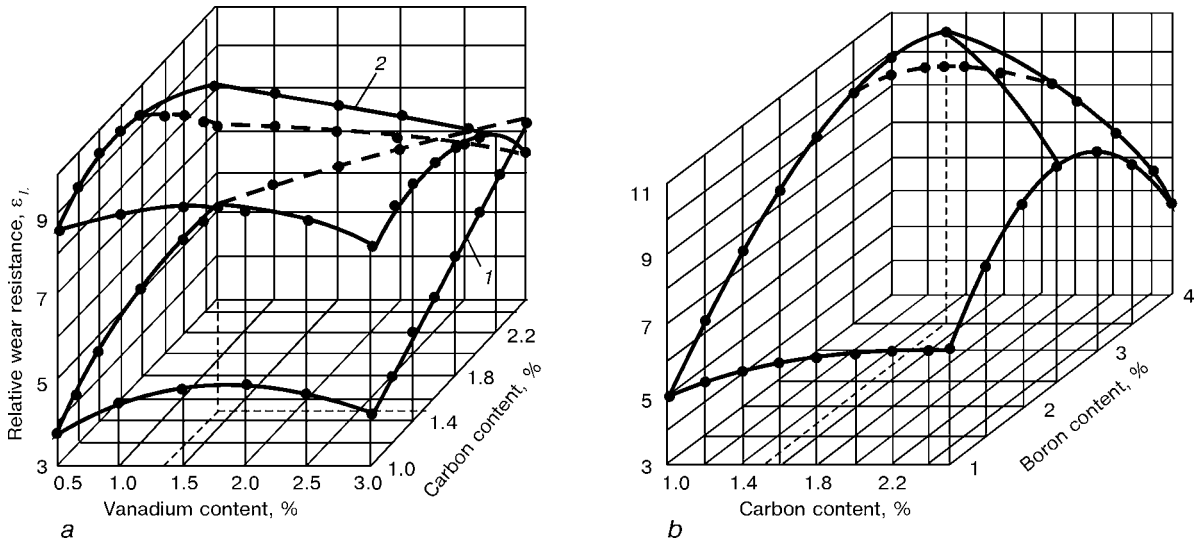

Figure 2. Effect of vanadium and carbon (*a*) at mass share of boron of 1.0 (*1*) and 3.5 % (*2*) and carbon and boron (*b*) at mass share of vanadium of 2.5 % on the relative wear resistance of deposited metal with 13 % of chromium

such as carbide formation and formation of boride phase which can suppress each other. At the lower level of boron (1 %) the wear resistance is determined mainly by the carbon content. This is associated with the fact that with increase in carbon from 1.0 to 2.5 % the amount of carbides of M_7C_3 type, carboborides $M_{23}(CB)_6$ and borocarbides $M_2(BC)$ is increased [7]. The main process in alloy crystallization is the formation of the carbide phase with boron atoms additionally introduced into its crystalline lattice, that causes the increase in hardness of inclusions and metal base and provides the increase in its wear resistance.

The dependence of the wear resistance on vanadium content at 13 % Cr and 1 % B has different forms. Thus, at mass share of carbon 2.5 % (ratio in atomic percentages V/C = 0.04 – 0.20) the alloy ability to resist the abrasive wear is increased monotonically, and at the mass share of carbon, equal to 1 % (ratio in atomic percentages V/C = 0.12 – 0.70), this dependence acquires a parabolic form with an extremum near 2 % concentration of vanadium (V/C = = 0.07). At a mass share of 3.5 % boron the dependence of wear resistance of the deposited metal on the mass shares of vanadium and carbon has a clearly expressed optimum in the region of content of 1.5 % C and 1.3 % V. As is seen in Figure 2, at optimum mass share of vanadium 1.3 % the dependence of wear resistance on the mass share of carbon and boron has a different nature. Thus, at minimum level of carbon (1 %) the increase in a mass share of boron from 1 to 4 % causes the monotonous growth of wear resistance. The increase in carbon content of higher than 1.5 % and that of boron of more than 3.5 % at optimum content of vanadium (1.3 %) leads to the decrease in the wear resistance.

The results of treatment of compositions of experimental alloys showed that the selected factors (carbon, boron, vanadium) and the levels of their varying make it possible to produce the deposited metal with a high wear resistance ($\varepsilon \geq 9$) depending on the values and mutual section of elements, that proves a proper selection of the alloying system. The analysis of the obtained relationships shows that the maximum value of relative wear resistance is attained at the following mass share of the deposited metal, %: Cr — 13.0; C — 1.5; B — 3.5, V — 1.3.

To check experimentally the wear-resistance of the produced alloy in the industrial conditions the samples of the deposited metal were tested. To avoid the random errors during wear, all the alloys of the matrix of the complete factorial experiment were tested together with the estimated alloy. The analysis of results of checking the wear resistance of the produced material showed a good correlation between the estimated and experimental data. The microstructure of the deposited metal and friction surface after service under the conditions of operation of the asphalt mixer agitators are presented in Figure 3.

The examination of structure of metal, deposited by the flux-cored wire PP-150Kh13R3F (C — 1.5; Cr — 13.0; W — 3.0; V — up to 1.0 wt.%; Fe —

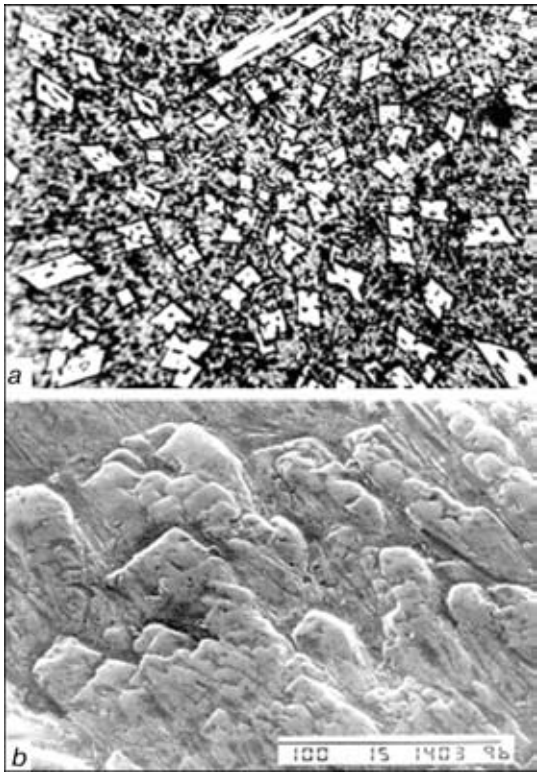

Figure 3. Microstructure (×300) of deposited metal of 150Kh13R3F type (*a*) and its friction surface after wear (×500) (*b*)

balance) showed that it consists of a comparatively soft martensitic-austenitic matrix and a large number (55 – 60 %) of strengthening phase of a high microhardness. The excessive phase has a shape of needles, distributed uniformly in the metal base, oriented at angles close to 90° with respect to the surface being deposited (Figure 3), as a major axis of boride needles coincides with the direction of heat removal and has a maximum rate of growth, thus suppressing the growth of crystals oriented at angle to the direction of heat removal [7]. This important quality of wear-resistant materials of the given system of alloying gives an opportunity to increase the ability of the alloy to the wear resistance, to provide the required orientation of the strengthening phase relative to the wear plane.

REFERENCES

1. Tenenbaum, M.M. (1976) *Wear resistance of structural materials and machine parts*. Moscow: Mashinostroyeniye.
2. Popov, S.N. (2000) Theoretical bases of multicriterial analysis of wear of steels and alloys. In: *Restoration and increase of wear resistance and service life of machine parts*. Zaporozhje: OAO Motor Sich.
3. Popov, S.N. (2000) Wear resistance of deposited metal of working elements of road-construction machines. *Avtomaticheskaya Svarka*, **8**, 15 – 20.
4. Brykov, N.N., Popov, S.N. (1991) Effect of structure of alloys of agitators of asphalt mixing machines on the wear resistance. *Stroit. i Dorozhn. Mashiny*, **2**, 18 – 19.
5. Livshits, L.S., Grinberg, N.A., Kurkummelli, E.G. (1989) *Fundamentals of deposited metal alloying*. Moscow: Machinostroyeniye.
6. Hartman, K., Letsky, E., Shefer, V. (1977) *Experiment planning in investigation of technological processes*. Moscow: Mir.
7. Popov, S.M. (2000) Peculiarities of effect of structure of hard inclusions on wear resistance of deposited heterogeneous alloys. *Metallovedeniye i Obrab. Metallov*, **3**, 21 – 25.

40 YEARS OF PILOTED COSMONAUTICS

Forty years ago just one turn around the globe was made... And we have every right to be proud that the pioneers of this event of world importance were our compatriots — academician Sergei Pavlovich Korolyev and Yuri Alekseevich Gagarin, Air Force Lieutenant.

In 1964 Boris Evgenievich Paton and Sergei Pavlovich Korolyev discussed the possibility of using manned space flights for staging and performance of fundamental materials science investigations in order to address scientific and applied goals of cosmonautics. This marked the beginning of space exploration for peaceful purposes.

Intensive development of space research involved the scientists and specialists of all fields of knowledge without exception, laid the foundations of new areas of science and technology. Over the last forty years, thousands of scientific reports, monographs and a great number of science fiction books were published, and hundreds of films were made, that are devoted to space subjects.

The editorial board was able to find the speech of Sergei Pavlovich Korolyev (Professor Sergeev) in March, before the launch of «Voskhod-2» vehicle. This was academician's last public speech. It needs no comments. It should be just noted that no science fiction writer in the world was able to foresee or forecast with one hundred percent accuracy the emergence of a new field of science, whereas Korolyev was able to do it.

Extract from S.P. Korolyev's speech in a press conference, March, 1965

Over the last few years, when so many space flights have been made, we are going over to a new quality, without noticing it. As you can see, first one-man vehicles were flying, now, three-man began to fly, and just now a two-men vehicle is going up. It can be said beforehand that one-man vehicles will hardly be flown any more. I believe I will not make any mistake, if I predict also the next step. It will soon be an issue that there is hardly any sense in launching such expensive systems as space vehicles for several days into space. They probably should be put into orbit and left there for quite a long time, and all the necessary supplies to these vehicles should be provided, and the crews should be delivered and replaced by using simplified types of space vehicles, which should certainly have a docking capability, so as to perform their functions, docking to a system of orbiting vehicles. This way we, without noticing it, are, as a matter of fact, advancing towards a qualitative change in our notions and areas of our work on space exploration, in the near space during orbital flights near the Earth so far. Now, speaking of longer term flights and longer range flights, you certainly understand that the vehicles cannot fly in such an independent manner that one vehicle can only have radio communication with another vehicle. Mutual assistance, reliability, duplication, whatever, even the very simplest human communication, are not an issue any more. Now, as regards why do we need leaving the vehicle, I believe this can be answered in a very simple manner, that, as a matter of fact, flying into space, man cannot help leaving the vehicles. Just as when going over the ocean, one cannot be afraid of falling overboard and not learn swimming.

This involves a whole number of operations that may be required when the vehicles meet. If required, this, by the way, greatly simplifies performance of special observations in space. And, finally, in those cases when something will need to be mended on the vehicle. **We are, for instance, seriously thinking that a cosmonaut who has made the exit into space, should be able to perform all the required repair-production operations, down to performance of welding, etc., etc**. This is not fantasy, this is a necessity.

The more people fly into space, the more acute will this need be. And, finally, we have to take into account the fact that eventually such a situation may arise when one vehicle should render assistance to another vehicle, but in what way then? The vehicles are highly protected structures in terms of thermal impact and, hence also strength. This means that one can approach a vehicle and, as a matter of fact, achieve nothing. For if it is just depressurized through the exit port, the people inside will be dead. Therefore, such a system of docking, life support and leaving the vehicle should be in place that would enable rendering such an assistance. At this point, we could fantasise a little, saying, for instance, that there can be especially large vehicles, that they maybe will not come up too close, may be even at tens of kilometers distance, they will be able to see each other, suppose due to radio engineering means. The question is how do we make the transfer from one vehicle to another one, probably, not in a space suit, after all, with an individual, let us say oxygen, and some kind of propulsion system. Then some kind of a space taxi, space boat is to be made for such a large distance. This is because both in terms of weight, and thermal characteristics and supplies of all kinds, safety, probably, it is not possible to let a man go as a grain of sand for, let us say, 20 km in space. It is better to make a taxi. He must have the capability of seeing his vehicle and the one where he is going, have the ability of returning to his vehicle and to the vehicle to which he is going, have communication with it, and all kinds of emergency duplication. So it is simpler, better to make such a lightweight piece, not bound by gravity, that will allow you to travel. (Applause.)

I can only refer your congratulations to a large team of developers and test engineers that have created and conducted this highly complicated experiment. I must say that the first exit of man into space is a major event in space research, I would say this is an event that will open up a large area in development of space vehicles and space research. That, as a matter of fact, is all that I wished to tell you.

The issues of the cosmonaut safety during work performance in raw space, in particular with hand tools, are given a lot of attention (see: Coll. of papers «Space: technologies, material science, structures». Ed. by B.E. Paton. Kiev: PWI, 2000). The hazard of working with the processing equipment consists in the damaging ability of the heat source (electron beam, arc discharge, exothermal mixtures, etc.). When preparing experiments with the hand electron beam welding tool, the hardware developers took into account the potential hazard of direct impact of the electron beam on the cover of the operator's space suit, as well as the space vehicle, outside which the operations were conducted and on its outer structures (aerials, solar batteries, etc.). Protection of the operator or the vehicle in these experiments was ensured by a thorough training of the operator, arranging his external work place, strict following of the instructions and procedures of the scheduled welding operations performance. However, both the hardware developers and specialists staging these complicated space experiments, realised very well that all the measures taken by them just partially lowered the level of the risk.

In 1998, upon the initiative of academician B.E. Paton, the scientific leader of the work on space welding technologies, a competition was announced on development of ideas (proposals) inexpensive and quite simple to carry out, embody in mock-ups and implement, for interlocking the electron beam when it goes beyond the working zone. A large team of specialists of both the E.O. Paton Electric Welding Institute and other organisations took part in the competition. It resulted in proposing the methods of «contouring» the working zone area with a current-conducting frame, or «painting» the working zone proper with a special dye-sensor; fitting the electron beam tool with a probe, providing electromechanical contact with the item being processed; incorporating into the hardware a device allowing probing with the electron beam the surfaces on which it impinges, or placing an infrared «beacon» on the item being welded; fitting the hardware with the video and radio location systems (AO «Kvant») or «technical vision». It was also proposed to consider the cosmonaut space suit as a kind of multilink manipulator (system of four manipulators — two arms and two legs — attached to a common base), fitted with angular displacement transducers in the junctions. (Unfortunately, this interesting proposal of Dr. F.N. Kisilevsky was received after the competition was over).

Three kinds of systems under the conditional titles of «Probing» (Yu.N. Lankin, and oth.), «Information beacon» (K.A. Bulatsev, and oth.), and «Technical vision» (V.V. Tochin, and oth.) were selected from the presented proposals for further development, making the mock-ups and conducting demonstration testing.

Given below are the papers that describe the implementation and results of testing performed in the laboratories of the E.O. Paton Electric Welding Institute, Ukraine, and J. Marshall Space Flight Center, NASA, USA, the experts of which M. Vanhooser, C. Russell, M. Terry and S. Clark have made a great contribution to preparation and performance of testing that is gratefully acknowledged by the authors of the published papers.

Editorial Board
Space Research Department

DEVICE FOR PROVISION OF SAFE OPERATION OF MANUAL ELECTRON BEAM TOOL IN SPACE

Yu.N. LANKIN and **S.S. GAVRISH**
The E.O. Paton Electric Welding Institute, NASU, Kyiv, Ukraine

ABSTRACT

A device for protection from the electron beam in manual electron beam welding in space is described. The device operation is based on short-term (0.002 s) probing with the electron beam of the surfaces being welded. When the distance from the gun to the surfaces being welded is increased above the working distance, the device lowers the beam power density to a safe level and (or) completely switches the beam off.

Key words: *space, hand tool, EBW, protection*

Functioning algorithm. If the electron beam gun is located at the working distance from the surface being processed (less than 150 mm) and the angle of the gun axis inclination is in the specified range ($90 \pm 30°$), work is performed with a standard sharply-focused beam. Every 0.5 s the electron beam probes the welding zone. Due to the very short probing time (2.25 ms) it does not in any way affect the technological properties of the beam.

If the distance from the gun to the surface which is hit by the beam is increased above the admissible level, the protection device will «blur» the electron beam. This will result in an abrupt lowering of the power density effectiveness, as well as of the damaging ability of the beam. The gun displacement into the working zone leads to restoration of the mode with the focused beam.

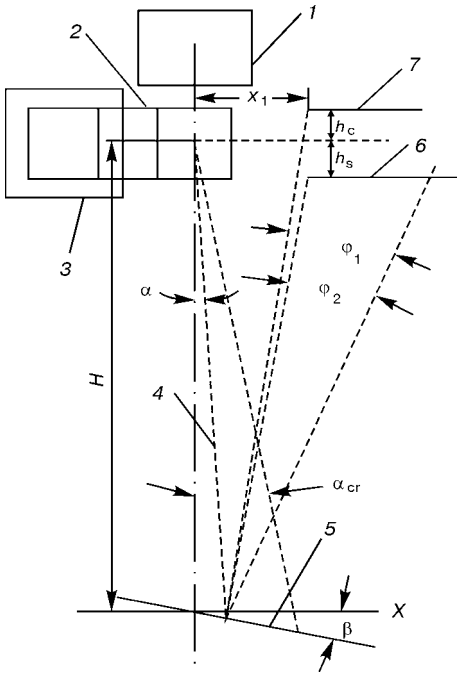

Figure 1. Schematic of beam trajectory in the device (for designations see the text)

Principle of operation. A standard electron beam gun *1* (Figure 1) is further fitted with an electromagnetic deflecting system, namely an open magnet core *2* and coil *3*. The electric current flowing through the coil, creates in the magnet core a magnetic field that deflects by angle α electron beam *4* injected by the gun. The coil current changes in time with 0.75 ms period by a saw-tooth law. This results in the beam changing from a point beam of 1.5 mm radius into a divergent linear beam. At 150 mm distance from the gun the beam width is ≈15 mm, i.e. the cross-sectional area is increased by about 13 times, and, therefore, the penetrability is decreased by the same number of times. With the increase of the distance from the gun to the surface, the power density of the periodically deflected beam decreases in inverse proportion to the distance.

Reflecting from processed surface *5*, part of the electron beam hits collector *7*. Screen *6* is mounted in front of it, due to which the collector current drops to zero at angle of deflection α_{cr}. As α_{cr} depends on distance H between the gun and the item, its value can be used for interlocking the beam when it leaves the working zone.

Let us study the dependence of collector current on system parameters and angle of deflection. Let us assume that the electron beam has a normal-circular distribution of current density in the cross-section

$$J = I_m \exp\left(-\frac{r^2}{2r_n^2}\right), \qquad (1)$$

where I_m is the current density amplitude; r is the distance from the beam axis in the plane normal to its axis; r_n is the beam «radius». Let us also assume that the electron trajectories are parallel and electron reflection from the surface follows the cosine law. Then, for the value of the electron flow to collector *7* we can write

$$I(\alpha) = I_m \int_0^{2\pi} \int_0^{\infty} \int_{\varphi_1}^{\varphi_2} \exp\left(-\frac{x^2 + y^2}{2r_n^2}\right) \cos\varphi \, d\gamma \, dr \, d\varphi, \quad (2)$$

where

$$\varphi_1 = \text{arctg}\left(\frac{x_1 - x(\alpha)}{y_1}\right) - \alpha - 2\beta;$$

$$\varphi_2 = \text{arctg}\left(\frac{x_1 - x(\alpha)}{y_2}\right) - \alpha - 2\beta;$$

$$x(\alpha) = K_1 \cos\alpha + x; \quad K_1 = H \frac{\text{tg}\,\alpha \sin(\pi/2 + \alpha)}{\sin(\pi/2 - \alpha - \beta)};$$

$$y_1 = H + h_c + K_1 \sin\alpha; \quad y_2 = H - h_s + K_1 \sin\alpha;$$

$$x = r \frac{\cos\gamma}{\cos(\alpha + \beta)}; \quad y = r \sin\alpha,$$

x_1 is the distance from the gun axis to the collector and screen; r and γ are the beam polar co-ordinates; β is the angle between the gun axis and normal to the item surface; H is the distance from the deflecting system to the item; h_c and h_s is the distance from the deflecting system center to the collector and screen.

Figure 2, *a* gives the calculated by (2) dependencies of collector current on the angle of the beam deflection for different distances from the gun to the reflecting surface. Similar dependencies are also found at the change of the angle of inclination β (Figure 2, *b*). One can see from the Figure that the critical angle of deflection of the electron beam is unambiguously connected with the distance to the reflecting surface and almost does not depend on the beam current value. On the other hand, the value of the collector current is directly proportional to the beam current and inversely proportional to the square of the distance. Therefore, with large distances from the gun to the reflecting surface, reflected electron signal is undetectable against the noise background. It is fortunate that this distance is essentially greater than the working distances and the absence of the collector current can be another signal for the electron beam interlocking.

Control module. The schematic of the control module is given in Figure 3. DD2 microprocessor generates an 8-digit code (port P1) that is converted by DAC (DA1 and DA2) into saw-tooth voltage. Power amplifier DA3 converts the saw-tooth voltage coming to its input, into the deflecting coil current. The negative current feedback is taken from resistor R6. A signal indicating the specified distance from the gun to the item, is formed at the output WR of microprocessor DD2. Green light-emitting diode VD1 is lit on the control module case. A signal of the electron beam interlocking is formed at the output RD. This signal is sent to the hand tool control panel. The signal coming from the collector is amplified by operational amplifier DA4. Potentiometer R14 is used to set the value of amplification by direct current, and potentiometer R10 — by alternating current. Comparator DA5, in which the operating level is set

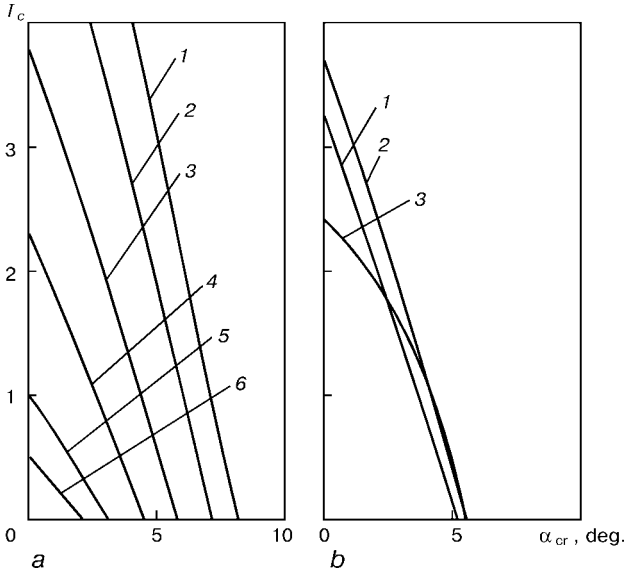

Figure 2. Dependence of collector current on the angle of electron beam deflection for different distances to the item (*a*): *1* — H = = 35; *2* — 40; *3* — 50; 4 — 65; *5* — 100; *6* — 150 mm, and for different angles of the gun inclination at H = 50 mm (*b*): *1* — β = = 0; *2* — 20; 3 — −20°

by potentiometer R15, generates rectilinear pulses of DA4 output voltage. These pulses are formed by level by diodes VD4, VD5 and come to inputs T1 and INTO of microprocessor DD2. The latter calculates the duration of these pulses during three periods of the electron beam deflection. If pulse duration is below 50 % of the deflection period, light-emitting diode VD1 is lit, and a logical unity appears at the output of microcircuit DD1.1. Generation of saw-tooth deflection current is interrupted. After 0.5 s three pulses of the electron beam deflection are generated again, collector current shape is analyzed, etc. Work is performed with the hand tool in the standard mode. The short time of probing the surface with the beam (3 × × 0.75 ms = 2.25 ms) and high repetition rate of the probing pulses (512 : 2.25 = 228) practically do not change the technological properties of the electron beam.

If the pulse duration at output DD5 over three periods of the beam deflection is greater than 50 % of the deflection period, the next three pulses of saw-tooth current are generated and so on. The beam being «blurred» because of periodical deviation at a high frequency, its penetrability falls abruptly, and the more the greater the distance to the surface onto which it drops. Light-emitting diode VD1 is not lit, after 4 s the signal (logical) for switching off the electron beam of 4 s duration, is generated at the output of microcircuit DD1.1. During this time the operator is to bring the gun back into the working zone. After 4 s the gun is switched on again. If it is in the working zone, then a standard mode will set in, after three deflection probing pulses. Otherwise, the beam will be «blurred» for 4 s and the beam switching on/off cycle will be repeated.

Experimental verification. The device mock-up was tested together with a set of «Universal» hard-

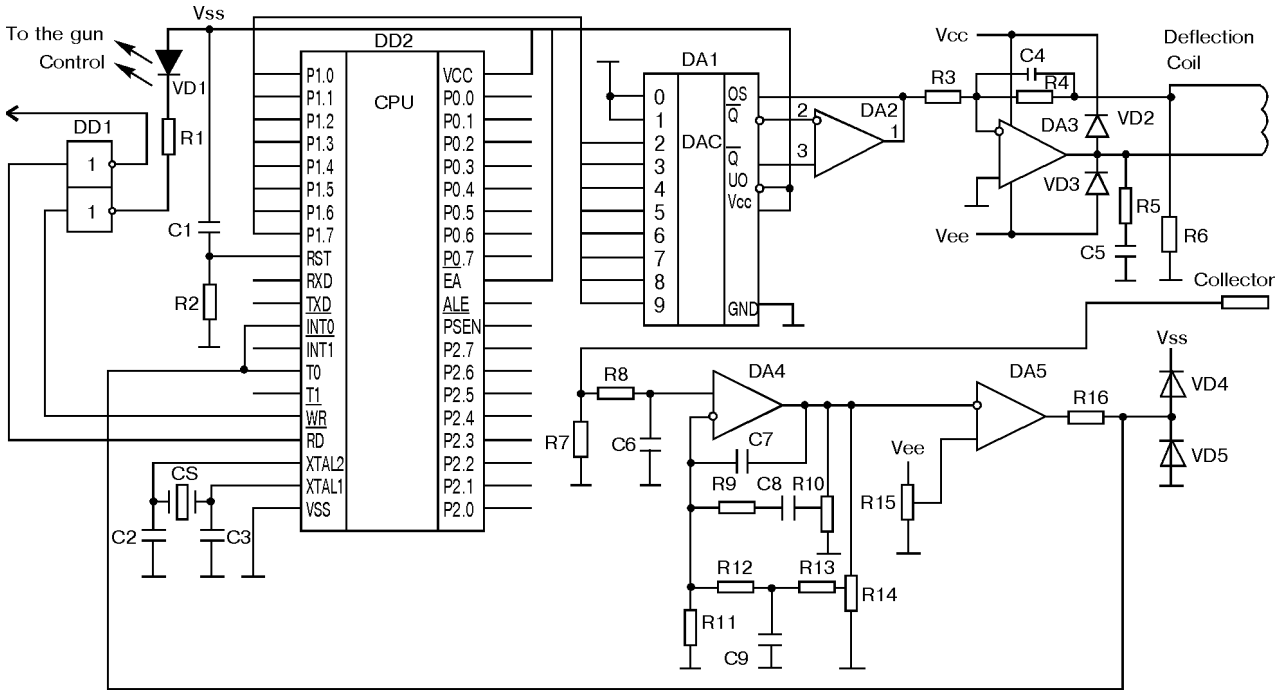

Figure 3. Simplified elementary diagram of the device

ware in simulation of manual EBW. The device was set up for operation at 55 – 65 mm distance from the gun to the stainless steel samples being welded. Beam current was set on the level of 55 mA. With this set up the influence of the change of the material being welded and the beam current value on the device operation was checked.

It was found that in welding of 304SS stainless steel and Ti–6Al–4V titanium alloy the protection operation range is 55 – 1000 mm at beam current of 55 – 75 mA. It is much narrower for aluminium alloy 2219 and for alloy 5456 it is 55 – 70 mm.

Thus, setting the device up on stainless steel provides guaranteed operation at an acceptable distance in welding of other materials.

With the change of the angle of the gun turning, as was assumed (Figure 2, *b*), protection operates when the electron beam goes beyond the board on which the samples are mounted, i.e. with a significant increase of the distance or at transition to the anodized surface of the board.

The working and «blurred» electron beam at protection device operation is given in Figure 4 (see color insert).

In conclusion, the advantages of the developed protection device should be noted, namely equipment simplicity, small weight and dimensions, reliability, insensitivity to environmental parameters (temperature, vacuum, vapour deposition, lighting, etc.). However, shortcomings of the device were also found during its operation, namely fitting the gun with the deflecting electromagnetic system with electron collector, that increase the gun overall dimensions; dependence of working zone parameters on the gun current value and processed surface material; the tested mock-up of the device does not protect the space suit material from damage at short range.

The device can be improved by introducing a correction by beam current up to complete elimination of the influence of the latter; improvement of the functioning algorithm and selection of setting up parameters to eliminate the possibility of the space suit burning through at any distance.

In the future the collector current of reflected electrons can be used for automatic correction of the electron beam position relative to the butt being welded, that will greatly improve the welding quality, as well as welding zone visualization.

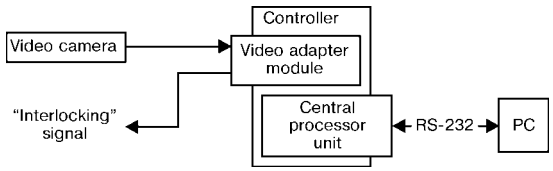

Figure 1. Functional diagram of the electron beam tool safety system

to the anode axis (adjustment) in the tool setting up. The parameters derived in setting, are entered into the controller working program, and thereafter it operates is a self-sufficient mode.

The principle of this system operation is based on finding the reference marks in the welding zone. The video camera is mounted on one axis with the tool anode. The video camera lens is aimed into the welding zone through a mirror (video camera optics protection). A control window is created by program means (see Figure 3 in the colour insert), inside which the check for reference marks is performed. The control window dimensions and its position in the frame, are assigned in setting up.

If three or more reference marks are within the control window when the tool is placed in the welding zone at the working distance from the sample, this is indicative of the tool being within the welding zone and is a sufficient condition for switching off the electron beam interlocking signal. If the number of reference marks in the control window is less than three or the marks are completely absent, a signal for the electron beam interlocking is given.

The algorithm of determination of the presence of reference marks in the control window is as follows:

- digital filtration of video information by brightness;
- creating the data matrix;
- searching for reference marks in the matrix by specified features;
- if the result is positive, eliminating the electron beam interlocking.

Mock-up testing of the above system of the electron beam tool interlocking as part of «Universal» hardware was conducted in a vacuum chamber fitted with a manipulator. The tool with the video camera was mounted on a manipulator, providing their displacement relative to the board with the samples to be welded. In addition to samples, the reference marks were also mounted on the board, that defined the working zone in which samples welding was to be performed. Observation of the electron beam switching on and off in the working zone and when the beam left the zone, was carried out at the tool displacement.

Testing was conducted with two kinds of reference marks, namely passive and active. Good lighting up of the welding zone was very important when working with passive marks (nonmetal circles painted black against a white background). The light sources were located on the tool and beyond it. When the tool was moved, the lighting of the welding zone was changed and the marks were partially lit up, while the light intervals between the marks were darkened, thus resulting in the change of the mark size and appearance of dark spots. The electron beam interlocking operated in the working zone. Since the work on selection of the correct lighting did not give positive results, an attempt was made to use active marks (light-emitting diodes, defining the working zone), the use of which yielded positive results. Selection of an appropriate level of black and white ratio allowed producing a rather stable image and forming the «allowing–interlocking» signal. When the tool left the welding zone, the interlocking signal switched the electron beam off. The melt zone in the welding area also was a light source. However, correct selection of the control zone eliminates the influence of this light source on taking a correct decision on interlocking.

When the electron beam was switched on during testing, interference appeared that, distorting the TV signal information, led to disappearance of the marks in the frame, as well as unauthorised (erroneous) interlocking of the electron beam. Interference, generated by inverter operation and electron beam «noise» confirmed the need for a more thorough investigation of the safety system protection from electromagnetic noise. The found faults and shortcomings of the above safety system did not permit us (unlike the first two proposals, published in this issue of the journal) taking it to demonstration testing stage, the terms of which were specified by the competition conditions.